Effects of Zeeman degeneracy on the steady-state properties of an atom interacting with a near-resonant laser field: Resonance fluorescence

Bo Gao
Department of Physics and Astronomy, University of Toledo, Toledo, Ohio 43606
(Received 10 February 1994)

Effects of the atomic Zeeman degeneracy on the resonance fluorescence spectrum of a closed two-level atom with arbitrary ground-state angular momentum J_g and excited-state angular momentum J_e are studied in detail. Especially interesting are the narrow structures due to the spontaneous Raman scattering and the incoherent Rayleigh scattering. Results for the cycling transition of a Cs atom are presented as part of the examples.

PACS number(s): 32.80.Pj, 42.50.Hz, 32.70.Jz

I. INTRODUCTION

Progresses in laser cooling and trapping have stimulated a great deal of interest in the effects of atomic Zeeman degeneracy on laser-atom interactions [1–20]. It has become quite clear that transitions with a degenerate ground state are in many aspects qualitatively different from a two-level system (TLS). With a degenerate ground state, laser-atom interactions become intrinsically nonperturbative (if ground-state m-changing collisions are insignificant) [21]. Polarization-gradient cooling becomes possible [1], and there can be structures which are much narrower than the spontaneous decay rate in both the probe [6–8,13,15,17,21] and the resonance fluorescence spectra [22,5,10,12,16,18, and this paper]. The significance of these studies is not limited to the laser cooling and trapping. After all, there is simply no atomic transition that can be strictly modeled as a TLS if the effects of collisions have to be taken into account [23].

This paper presents a systematic study of the effects of the atomic Zeeman degeneracy on the resonance fluorescence spectrum. Atomic motion is ignored. The narrow resonances which are due to the localized atomic motion [5,10,12,16,18] will, therefore, not be discussed. The system we consider is a two-level stationary atom with arbitrary ground-state angular momentum J_g and excited-state angular momentum J_e interacting with a linearly polarized coherent laser field. We show how the resonance fluorescence spectrum for such a system can be calculated easily and efficiently for any detuning and Rabi frequency. Results for degenerate transitions ($J_g \neq 0$) are found to differ qualitatively from the spectrum of a TLS ($J_g = 0$ and $J_e = 1$) [24]. For example, it is well known that the resonance fluorescence of a TLS is completely coherent in the limit of either weak field or large detuning [24]. This is found not to be the case for Zeeman-degenerate transitions. The origin of this difference will be traced to the spontaneous Raman scattering and the incoherent Rayleigh scattering, both of which show up as narrow structures in the spectrum when the laser-atom coupling is relatively weak. Another key difference due to the Zeeman degeneracy is the frequency dependence of the angular distribution. For a TLS, the angular distribution is frequency independent because the resonance fluorescence comes solely from the $\Delta m = 0$ type of processes. In contrast, there are three types of processes with $\Delta m = 0, +1$, and -1 that contribute to the resonance fluorescence of a Zeeman-degenerate transition. The angular distribution is determined by their *relative* contributions which can obviously be frequency dependent. Among Zeeman-degenerate transitions, we will also address the differences between the $\Delta J = 0$ and the $\Delta J = 1$ types of transitions [25].

Our procedure for calculating the resonance fluorescence spectrum is based on the approach of Ref. [26] (referred thereafter as paper I) in which the analytic solution for the steady-state density matrix is derived. This approach emphasizes the following points which are completely independent of the particular system we are studying. First, the resolvent operator (in the Liouville space) contains *all* the information embedded in the original master equation, including the steady-state density matrix elements which are related to the residues of the resolvent operator [26]. This is not surprising since the resolvent operator is the Laplace transform of the time evolution operator for the master equation. Second, for a system of finite dimensions the computation of the resolvent operator requires only a matrix inversion. Third, symmetry can greatly simplify the computation. These simple realizations are crucial for achieving the kind of generality we are looking for.

II. THEORY

A. Resonance fluorescence spectrum and its angular distribution

The theory presented here is a generalization of the work of Mollow [24] to transitions between states of arbitrary angular momenta. The derivation of the resonance fluorescence spectrum is the same as that presented in Ref. [27] and I will simply give the result for a stationary atom,

$$W_{\mathbf{e}}(\omega,\theta,\phi)=\left(\frac{k_{eg}^3}{2\pi^2\hbar}\right)\lim_{\eta\to 0+}\mathrm{Re}\Big\{\mathrm{Tr}_A(\mathbf{e}^*\cdot\boldsymbol{\mu}^-) \times R(\eta-i(\omega-\omega_L))\left[\rho_A^{\mathrm{SS},R}(\mathbf{e}\cdot\boldsymbol{\mu}^+)\right]\Big\}\ . \quad (1)$$

Here $W_{\mathbf{e}}(\omega,\theta,\phi)$ is defined such that $W_{\mathbf{e}}(\omega,\theta,\phi)d\omega d\Omega$ is the rate of emitting a photon with polarization $\mathbf{e}$ and frequency inside $d\omega$ into a solid angle $d\Omega$. $\mu^{\pm}$ are the atomic raising and lowering dipole operators, respectively. $R(s)$ is the resolvent operator defined by

$$R(s)\equiv\left(s-L_A^R\right)^{-1}\ ,$$

in which L_A^R is the Liouville operator of the density matrix equation in the rotating frame and rotating-wave approximation (RWA). And $\rho_A^{\mathrm{SS},R}$ is the corresponding steady-state density matrix. For a J_g to J_e transition driven by a linearly polarized coherent laser field,

$$\mathbf{E}(t)=E_0\hat{\mathbf{z}}\cos\omega_L t\ ,$$

the density matrix equation in the rotating frame and RWA is given by [28]

$$\begin{aligned}\partial_t\rho_A^R(t)&=L_A^R\rho_A^R(t)\\&=(1/i\hbar)\left[\left(H_A^R+H_{AL}^R\right),\ \rho_A^R(t)\right]-(\gamma/2)\sum_{m_e}|J_e m_e\rangle\langle J_e m_e|\rho_A^R(t)-\rho_A^R(t)(\gamma/2)\sum_{m_e}|J_e m_e\rangle\langle J_e m_e|\\&\quad+\gamma\sum_{q,\ \text{all}\ m}\langle J_g m_g' 1q|J_e m_e'\rangle|J_g m_g'\rangle\langle J_e m_e'|\rho_A^R(t)|J_e m_e\rangle\langle J_g m_g|\langle J_g m_g 1q|J_e m_e\rangle\ ,\end{aligned} \quad (2)$$

with

$$H_A^R=-\hbar\Delta\sum_{m_e}|J_e m_e\rangle\langle J_e m_e|\ , \quad (3)$$

and

$$H_{AL}^R=-\hbar(\Omega_{eg}/2)\sum_m f_m(|J_e m\rangle\langle J_g m|+|J_g m\rangle\langle J_e m|)\ , \quad (4)$$

where $\Delta=\omega_L-\omega_{eg}$ is the laser detuning;

$$\gamma\equiv\frac{4}{3\hbar}k_{eg}^3\frac{|\langle J_e||\mu||J_g\rangle|^2}{2J_e+1} \quad (5)$$

and

$$\Omega_{eg}\equiv E_0\langle J_e||\mu||J_g\rangle/\hbar \quad (6)$$

are, respectively, the spontaneous decay rate of the excited state and the reduced Rabi frequency; and

$$f_m\equiv(-1)^{J_e-m}\begin{pmatrix}J_e & 1 & J_g\\ -m & 0 & m\end{pmatrix}\ .$$

We have obviously taken the laser polarization as the quantization axis in defining our m states.

It is convenient to introduce $W_q(\omega)$ $(q=-1,0,1)$ defined by [29]

$$W_q(\omega)\equiv W_{\mathbf{e}=\boldsymbol{\epsilon}_q}=\left(\frac{k_{eg}^3}{2\pi^2\hbar}\right)\lim_{\eta\to 0+}\mathrm{Re}\Big\{\mathrm{Tr}_A(\boldsymbol{\epsilon}_q^*\cdot\boldsymbol{\mu}^-) \times R(\eta-i(\omega-\omega_L))\left[\rho_A^{\mathrm{SS},R}(\boldsymbol{\epsilon}_q\cdot\boldsymbol{\mu}^+)\right]\Big\} \quad (7)$$

where $\boldsymbol{\epsilon}_0=\hat{\mathbf{z}}$; $\boldsymbol{\epsilon}_1=-(1/\sqrt{2})(\hat{\mathbf{x}}+i\hat{\mathbf{y}})$; $\boldsymbol{\epsilon}_{-1}=(1/\sqrt{2})(\hat{\mathbf{x}}-i\hat{\mathbf{y}})$. They can be written as

$$W_0(\omega)=\left[\frac{3(2J_e+1)\gamma}{8\pi^2}\right]\sum_{mm'}f_m f_{m'}\lim_{\eta\to 0+}\mathrm{Re}\Big\{\langle m|R_{eg,gg}^{(0)}(\eta-i(\omega-\omega_L))|m'\rangle\langle J_g m'|\rho_A^{\mathrm{SS},R}|J_e m'\rangle +\langle m|R_{eg,eg}^{(0)}(-i(\omega-\omega_L))|m'\rangle\langle J_e m'|\rho_A^{\mathrm{SS},R}|J_e m'\rangle\Big\}\ , \quad (8)$$

$$W_1(\omega)=\left[\frac{3(2J_e+1)\gamma}{8\pi^2}\right]\sum_{mm'}h_m h_{m'}\mathrm{Re}\Big\{\langle m|R_{eg,gg}^{(1)}(-i(\omega-\omega_L))|m'\rangle\langle J_g m'|\rho_A^{\mathrm{SS},R}|J_e m'\rangle +\langle m|R_{eg,eg}^{(1)}(-i(\omega-\omega_L))|m'\rangle\langle J_e m'|\rho_A^{\mathrm{SS},R}|J_e m'\rangle\Big\}\ , \quad (9)$$

and $W_{-1}(\omega) = W_1(\omega)$ in the absence of any magnetic field. Here $\langle m|R^{(l)}_{ab,cd}(s)|m'\rangle$ is defined by

$$\langle m|R^{(l)}_{ab,cd}(s)|m'\rangle \equiv \langle\langle am, bm-l|R(s)|cm', dm'-l\rangle\rangle \ , \tag{10}$$

which can be calculated easily for any transition using the method of paper I (see also Appendix A). And h_m is defined by

$$h_m \equiv (-1)^{J_e-m}\begin{pmatrix} J_e & 1 & J_g \\ -m & 1 & m-1 \end{pmatrix} .$$

$\rho_A^{SS,R}$ is the steady-state solution of Eq. (2) for which a simple analytic formula is available in paper I. m and m' are summed from $-J_g$ to $+J_g$ in Eq. (8) and from $-J_g+1$ to $+J_g$ in Eq. (9). In going from Eq. (7) to Eqs. (8) and (9), we have used the fact that the representation of the resolvent operator R in the Liouville space $|J_1m_1, J_2m_2\rangle\rangle$ is block diagonal in $l \equiv m_1 - m_2$, which is a direct consequence of the cylindrical symmetry (paper I and Appendix A).

W_qs are introduced not only because it make sense computationally (to take advantage of the cylindrical symmetry), but also because they are associated separately with processes in which the change of magnetic quantum number Δm is $-q$, greatly facilitating physical interpretations (the minus sign arise because we are dealing with emissions). For example, the Rayleigh scattering, with $\Delta m = 0$, contributes only to $W_0(\omega)$, while the spontaneous Raman scattering, with $|\Delta m| = 1$, contributes only to $W_{\pm1}(\omega)$.

By expanding $\mathbf{e}$ in terms of ϵ_qs, the spectrum for emitting a photon of an arbitrary polarization can be written in terms of W_qs. Letting $\hat{\mathbf{k}}$ be the unit k vector for the emitted photon, the double differential rates for emitting a photon with polarizations $\mathbf{e}_\perp = \hat{\mathbf{k}}\times\hat{\mathbf{z}}/|\hat{\mathbf{k}}\times\hat{\mathbf{z}}|$ and $\mathbf{e}_\parallel = \mathbf{e}_\perp \times \hat{\mathbf{k}}$ are given, respectively, by

$$\begin{aligned}\frac{d^2W_\perp}{d\omega d\Omega} &\equiv W_\perp(\omega,\theta,\phi) \\ &= \tfrac{1}{2}[W_1(\omega)+W_{-1}(\omega)] \ ,\end{aligned} \tag{11}$$

which is isotropic, and

$$\begin{aligned}\frac{d^2W_\parallel}{d\omega d\Omega} &\equiv W_\parallel(\omega,\theta,\phi) \\ &= W_0(\omega)\sin^2\theta + \tfrac{1}{2}[W_1(\omega)+W_{-1}(\omega)]\cos^2\theta \ .\end{aligned} \tag{12}$$

The unit vectors $\mathbf{e}_\parallel$, $\mathbf{e}_\perp$, and $\hat{\mathbf{k}}$ are defined in such a way that $\mathbf{e}_\parallel$ is parallel to the plane of $\hat{\mathbf{k}}$ and $\hat{\mathbf{z}}$, $\mathbf{e}_\perp$ is perpendicular to this plane, and $\mathbf{e}_\parallel \times \mathbf{e}_\perp = \hat{\mathbf{k}}$. The double differential rate summed over photon polarization is, therefore,

$$\begin{aligned}\frac{d^2W}{d\omega d\Omega} &\equiv W(\omega,\theta,\phi) \\ &= W_0(\omega)\sin^2\theta + \tfrac{1}{2}[W_1(\omega)+W_{-1}(\omega)](1+\cos^2\theta) \ .\end{aligned} \tag{13}$$

The angular distributions of $W_\parallel$, $W_\perp$, and W are all independent of ϕ because of the cylindrical symmetry.

We have kept both $W_1(\omega)$ and $W_{-1}(\omega)$ [$=W_1(\omega)$] in Eqs. (11)–(13) so that they would remain valid even when there is a magnetic field parallel to the direction of the laser polarization, in which case we still have a cylindrical symmetry, but $W_1(\omega)$ and $W_{-1}(\omega)$ would no longer be equal.

$W_\parallel(\omega,\theta,\phi)$, $W_\perp(\omega,\theta,\phi)$, and $W(\omega,\theta,\phi)$ are what the experiment can measure directly. From Eqs. (11)–(13), it is clear that such measurements can be used to determine both $W_0(\omega)$ and $W_1(\omega)$ [$=W_{-1}(\omega)$]. This can be accomplished either by measuring both $W_\parallel(\omega,\theta,\phi)$ and $W_\perp(\omega,\theta,\phi)$ at a single angle $\theta \neq 0$, e.g., $\theta = \pi/2$, or by measuring $W(\omega,\theta,\phi)$ at two different angles, e.g., $\theta = 0$ and $\theta = \pi/2$. The motivation for determining both $W_0(\omega)$ and $W_1(\omega)$ is that it enables us to look at the contributions to the resonance fluorescence from $\Delta m = 0$ and $|\Delta m| = 1$ types of processes separately.

The coherent part of the spectrum can be singled out explicitly. Only $W_0(\omega)$ has a coherent component since as is shown in paper I, only $R^{(0)}_{eg,gg}(s)$ has a $1/s$ pole. Using the relation

$$\lim_{s\to0} s\langle\langle i,j|R(s)|m,n\rangle\rangle = \langle i|\rho^{SS}|j\rangle\delta_{mn} \ , \tag{14}$$

and the analytic formula for the steady-state density matrix $\rho_A^{SS,R}$ (both of which are derived in paper I), we obtain

$$W_0(\omega) = W_{0,\mathrm{coh}}(\omega) + W_{0,\mathrm{inc}}(\omega) \ , \tag{15}$$

with

$$\begin{aligned}W_{0,\mathrm{coh}}(\omega) = (3/8\pi)(2J_e+1)\gamma&\left(g_s^2\Omega_{eg}^2/4\right) \\ &\times\left[\Delta^2+(\gamma/2)^2\right]\left[\Delta^2+(\gamma/2)^2\right. \\ &\left.+g_s\Omega_{eg}^2/2\right]^{-2}\delta(\omega-\omega_L) \ ,\end{aligned} \tag{16}$$

where [26]

$$g_s \equiv \sum_{m'=-J_g}^{J_g} w_{m'} f_{m'}^2 \ , \tag{17}$$

$$w_m \equiv \chi_m\left(\sum_{m'=-J_g}^{J_g}\chi_{m'}\right)^{-1} \ , \tag{18}$$

$$\chi_m \equiv \left(\prod_{m'=-m+1}^{J_g} f_{m'}^2 h_{m'}^2\right)\left(\prod_{m''=m+1}^{J_g} f_{m''}^2 h_{m''}^2\right) \ . \tag{19}$$

(The definition of χ_m can be changed by any multiplication constant without affecting w_m.) $W_{0,\mathrm{inc}}(\omega)$ is determined by setting $\eta = 0$ in Eq. (8), which can then be calculated following the procedure of Appendix A.

Equations (11)–(13), along with Eqs. (15) and (16), can also be written as

$$W_{\parallel}(\omega,\theta,\phi) = W_{\rm coh}(\omega,\theta,\phi) + W_{\parallel,\rm inc}(\omega,\theta,\phi)$$
$$= \frac{W_{\rm coh}(\omega)}{4\pi}\left[1+\beta_{\rm coh}P_2(\cos\theta)\right] + \frac{W_{\parallel,\rm inc}(\omega)}{4\pi}\left[1+\beta_{\parallel,\rm inc}(\omega)P_2(\cos\theta)\right], \quad (20)$$

$$W_{\perp}(\omega,\theta,\phi) = \frac{W_{\perp}(\omega)}{4\pi}\left[1+\beta_{\perp}(\omega)P_2(\cos\theta)\right], \quad (21)$$

$$W(\omega,\theta,\phi) = W_{\rm coh}(\omega,\theta,\phi) + W_{\rm inc}(\omega,\theta,\phi)$$
$$= \frac{W_{\rm coh}(\omega)}{4\pi}\left[1+\beta_{\rm coh}P_2(\cos\theta)\right] + \frac{W_{\rm inc}(\omega)}{4\pi}\left[1+\beta_{\rm inc}(\omega)P_2(\cos\theta)\right], \quad (22)$$

where $P_2(x) = (3x^2-1)/2$ is the second order Legendre polynomial, and

$$W_{\rm coh}(\omega) = (2J_e+1)\gamma\left(g_s^2\Omega_{eg}^2/4\right)\left[\Delta^2+(\gamma/2)^2\right] \times\left[\Delta^2+(\gamma/2)^2+g_s\Omega_{eg}^2/2\right]^{-2}\delta(\omega-\omega_L), \quad (23)$$

$$\beta_{\rm coh} = -1, \quad (24)$$

$$W_{\parallel,\rm inc}(\omega) = (2\pi/3)\left[4W_{0,\rm inc}(\omega)+W_1(\omega)+W_{-1}(\omega)\right], \quad (25)$$

$$\beta_{\parallel,\rm inc}(\omega) = 2\left[W_1(\omega)+W_{-1}(\omega)-2W_{0,\rm inc}(\omega)\right] \times\left[4W_{0,\rm inc}(\omega)+W_1(\omega)+W_{-1}(\omega)\right]^{-1}, \quad (26)$$

$$W_{\perp}(\omega) = 2\pi\left[W_1(\omega)+W_{-1}(\omega)\right], \quad (27)$$

$$\beta_{\perp} = 0, \quad (28)$$

$$W_{\rm inc}(\omega) = W_{\parallel,\rm inc}(\omega)+W_{\perp}(\omega) = (8\pi/3)\left[W_{0,\rm inc}(\omega)+W_1(\omega)+W_{-1}(\omega)\right], \quad (29)$$

$$\beta_{\rm inc}(\omega) = (1/2)\left[W_1(\omega)+W_{-1}(\omega)-W_{0,\rm inc}(\omega)\right] \times\left[W_{0,\rm inc}(\omega)+W_1(\omega)+W_{-1}(\omega)\right]^{-1}. \quad (30)$$

The physical meanings of various quantities are quite clear. For example, $W_{\rm inc}(\omega)$ is defined such that it is related to $W_{\rm inc}(\omega,\theta,\phi)$ by

$$W_{\rm inc}(\omega) = \int d\Omega W_{\rm inc}(\omega,\theta,\phi) = \frac{dW_{\rm inc}}{d\omega}. \quad (31)$$

Similar relationships hold between $W_{\rm coh}(\omega)$ and $W_{\rm coh}(\omega,\theta,\phi)$, and between $W_{\perp}(\omega)$ and $W_{\perp}(\omega,\theta,\phi)$. We will also use $W(\omega)$ defined by

$$W(\omega) \equiv \frac{dW}{d\omega} = \int d\Omega W(\omega,\theta,\phi) = (8\pi/3)[W_0(\omega)+W_1(\omega)+W_{-1}(\omega)] = W_{\rm coh}(\omega)+W_{\rm inc}(\omega). \quad (32)$$

From Eqs. (12)–(13), (26) and (30), it is clear that the angular distributions of $W_{\parallel}$ and W are determined by the relative contributions from $\Delta m = 0$ and $|\Delta m| = 1$ types of processes. As far as rates summed over photon polarizations (W, $W_{\rm coh}$, and $W_{\rm inc}$) are concerned, the generic angular distribution for $\Delta m = 0$ type of processes is $(3/8\pi)\sin^2\theta$, corresponding to $\beta = -1$, and the generic angular distribution for $|\Delta m| = 1$ type of processes is $(3/16\pi)(1+\cos^2\theta)$, corresponding to $\beta = 1/2$. The angular distributions of W and $W_{\rm inc}$ are generally mixtures of these two weighted by the relative contributions from $\Delta m = 0$ and $|\Delta m| = 1$ types of processes. $\beta_{\rm coh} = -1$ because only the processes of the type $\Delta m = 0$ contribute to the coherent (Rayleigh) scattering.

Complete characterization of the resonance fluorescence spectrum has thus been reduced to calculating $W_{0,\rm inc}(\omega)$ [Eq. (8) with η set to zero] and $W_1(\omega)$

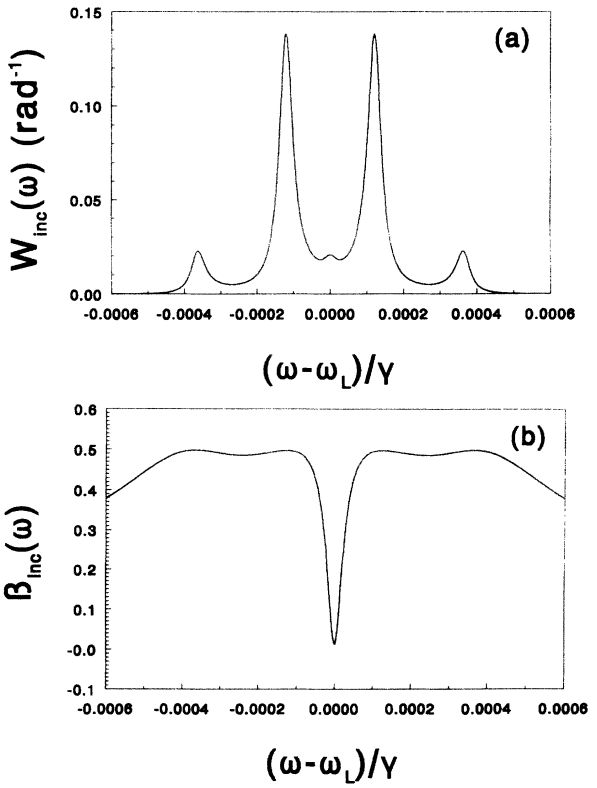

FIG. 1. (a)$W_{\rm inc}(\omega)$ for a $J_g = 2$ to $J_e = 3$ transition with $\Delta = -20\gamma$ and $\Omega_{eg} = 1.01246\gamma$ ($S = 10^{-4}$). (b) The corresponding β parameter $\beta_{\rm inc}(\omega)$.

$[W_{-1}(\omega) = W_1(\omega)]$, which can be accomplished by using Eqs. (8) and (9) and the techniques presented in Appendix A for computing the resolvent operator. Figure 1 is the result for a $J_g = 2$ to $J_e = 3$ transition with parameters $\Delta = -20\gamma$, $\Omega_{eg} = 1.01246\gamma$. Note that all resonances in this figure have widths much smaller than the spontaneous decay rate γ. No such narrow resonance exists in the spectrum of a TLS [24]. The questions are, therefore, where do these resonances come from and why are they so narrow? Section II B, along with Appendices B and C, addresses these questions.

B. Sum rules

A number of sum rules are presented in this section. They play an important role in our understanding of the resonance fluorescence spectrum by providing a link between our results and the predictions of the usual wave function perturbation theory. As noted in Ref. [21], even though the laser-atom interaction becomes intrinsically nonperturbative for transitions with a degenerate ground state (so that strictly speaking the wave function perturbation theory cannot be counted on to predict the line shapes no matter how weak the laser intensity is), the wave function perturbation theory still works for integrated rates as long as the laser-atom coupling is weak. This is important because regardless of its limitations, the traditional wave function perturbation theory still provides the best way to visualize physical processes. This section demonstrates how the wave function perturbation theory can help us to understand the origins of the narrow structures in the resonance fluorescence spectrum.

Using the relation

$$\lim_{\eta\to 0+}\int d\omega[\eta - i(\omega-\omega_L) - L_A^R]^{-1} = \pi I\ , \tag{33}$$

where I is a unit operator in the Liouville space, and the analytic formula for the steady-state density matrix [26], it is straightforward to show from Eq. (7) that

$$\begin{aligned} W_0 &\equiv \int d\omega W_0(\omega) \\ &= (3/8\pi)(2J_e+1)g_4\gamma\left(\Omega_{eg}^2/4\right) \\ &\quad\times\left[\Delta^2 + (\gamma/2)^2 + g_s\Omega_{eg}^2/2\right]^{-1}\ , \end{aligned} \tag{34}$$

$$\begin{aligned} W_1 &\equiv \int d\omega W_1(\omega) \\ &= (3/16\pi)\left[g_s - (2J_e+1)g_4\right]\gamma\left(\Omega_{eg}^2/4\right) \\ &\quad\times\left[\Delta^2 + (\gamma/2)^2 + g_s\Omega_{eg}^2/2\right]^{-1} \end{aligned} \tag{35}$$

$$\begin{aligned} W_{-1} &\equiv \int d\omega W_{-1}(\omega) \\ &= W_1\ , \end{aligned} \tag{36}$$

where we have defined

$$g_4 \equiv \sum_{m=-J_g}^{J_g} w_m f_m^4\ . \tag{37}$$

Various sum rules can be easily derived from these three. For $W(\omega)$, we obtain from Eq. (32)

$$W \equiv \int d\omega W(\omega) = \gamma P_e\ , \tag{38}$$

where P_e is the total population in the excited state and is given by [26]

$$\begin{aligned} P_e &\equiv \sum_m \langle J_e m|\rho_A^{SS,R}|J_e m\rangle \\ &= \left(g_s\Omega_{eg}^2/4\right)\left[\Delta^2 + (\gamma/2)^2 + g_s\Omega_{eg}^2/2\right]^{-1}\ , \end{aligned} \tag{39}$$

in which g_s [Eq. (17)] can be regarded as a parameter characterizing the rigidity of a transition, in the sense that for two transitions with the same decay rate and reduced dipole moment $\langle J_e||\mu||J_g\rangle$, the one with smaller g_s requires a larger laser intensity to excite. A table for g_s can be found in paper I. More data are gathered in Fig. 2 on two branches: one for $\Delta J = 0$ type of transitions and one for $\Delta J = 1$ type of transitions [25]. We can, therefore, say that $\Delta J = 0$ type of transitions are more rigid (harder to excite) than $\Delta J = 1$ type of transitions, and the rigidity increases with J_g for both types of transitions. It then becomes obvious that Ω_{eg} by itself is not an accurate representation of the laser-atom coupling strength. A better parameter for this purpose is the saturation parameter defined by

$$S = \left(g_s\Omega_{eg}^2/2\right)\left[\Delta^2 + (\gamma/2)^2\right]^{-1}\ . \tag{40}$$

With this definition, the total excited-state population is simply

$$P_e = \tfrac{1}{2}S(1+S)^{-1}\ . \tag{41}$$

And $S = 1$ corresponds to $P_e = 1/4$. The importance of the saturation parameter S lies in the fact that all integrated rates [Eqs. (34)–(36), (38), (42)–(43), and (45)–(46)], when scaled by γ, depend on Δ, Ω_{eg}, and γ only

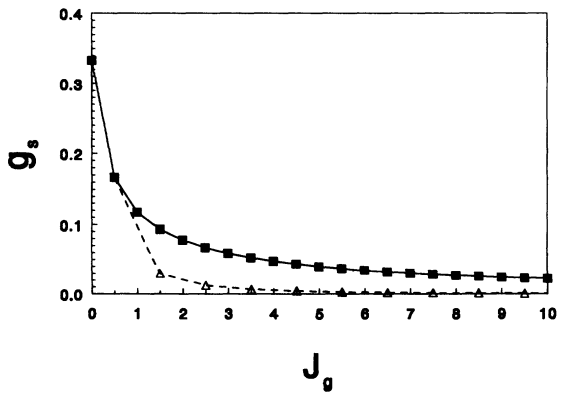

FIG. 2. g_s vs J_g. Solid squares are for $\Delta J = 1$ type of transitions. Triangles are for $\Delta J = 0$ type of transitions. Lines are drawn to guide the eyes.

through S [Appendix B].

The sum rule for the coherent part of the spectrum comes directly from Eq. (23),

$$W_{\rm coh} \equiv \int d\omega W_{\rm coh}(\omega) = (2J_e+1)\gamma\left(g_s^2\Omega_{eg}^2/4\right)\left[\Delta^2+(\gamma/2)^2\right] \times\left[\Delta^2+(\gamma/2)^2+g_s\Omega_{eg}^2/2\right]^{-2} . \quad (42)$$

The sum rule for the incoherent part of the spectrum is, therefore,

$$W_{\rm inc} \equiv \int d\omega W_{\rm inc}(\omega) = \gamma\left(g_s\Omega_{eg}^2/4\right)\left\{\left[1-(2J_e+1)g_s\right] \times\left[\Delta^2+(\gamma/2)^2\right]+g_s\Omega_{eg}^2/2\right\} \times\left[\Delta^2+(\gamma/2)^2+g_s\Omega_{eg}^2/2\right]^{-2} . \quad (43)$$

Here we see one of the major differences between a transition with a degenerate ground state ($J_g \neq 0$) and a TLS: in the limit of weak coupling $S \to 0$ (due to either weak field or large detuning), the resonance fluorescence of a degenerate transition ($J_g \neq 0$) is *not* completely coherent. In fact, defining

$$p_{\rm inc}(J_g, J_e) \equiv 1-(2J_e+1)g_s ,$$

we have in the limit of weak coupling ($S \to 0$),

$$W_{\rm inc}/W = p_{\rm inc}(J_g, J_e) + O(S) . \quad (44)$$

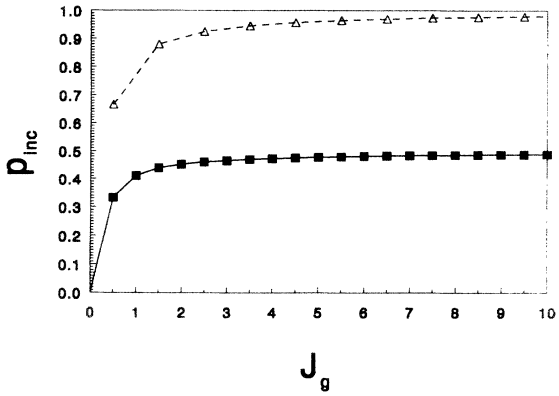

FIG. 3. $p_{\rm inc}(J_g, J_e)$ vs J_g. Solid squares are for $\Delta J = 1$ type of transitions. Triangles are for $\Delta J = 0$ type of transitions. Lines are drawn to guide the eyes.

$p_{\rm inc}(J_g, J_e)$ is, therefore, the fraction of incoherent scattering in the limit of weak coupling. Table I lists this parameter for all transitions of interest up to $J_g = 4$ to $J_e = 5$. More data are shown in Fig. 3 on two branches with $\Delta J = 0$ and $\Delta J = 1$, respectively [25]. The incoherent scattering in the limit of the weak coupling is clearly very significant for all transitions except the equivalent of a TLS: $J_g = 0$ to $J_e = 1$. This is especially true for transitions with $J_e = J_g$ and equal to a half integer, for which the laser-atom scattering (even in the limit of weak coupling) become almost 100% incoherent for large J_g. For $J_e = J_g + 1$ type of transitions, the laser-atom scattering in the limit of weak coupling is about 50% incoherent for large J_g.

The origin of this incoherent part can be understood by writing out the contributions to $W_{\rm inc}$ from $\Delta m = 0$ type of processes and $|\Delta m| = 1$ type of processes separately [see Eq. (29)]. From Eqs. (34) and (16), we obtain the contribution to $W_{\rm inc}$ from the $\Delta m = 0$ type of processes:

$$W_{\rm inc}^{\Delta m=0} \equiv (8\pi/3)\int d\omega W_{0,\rm inc}(\omega) = (8\pi/3)\left[W_0 - \int d\omega W_{0,\rm coh}(\omega)\right] = (2J_e+1)\gamma\left(\Omega_{eg}^2/4\right)\left[\Delta^2+(\gamma/2)^2+g_s\Omega_{eg}^2/2\right]^{-2}\left\{\left(g_4-g_s^2\right)\left[\Delta^2+(\gamma/2)^2\right]+g_sg_4\Omega_{eg}^2/2\right\} . \quad (45)$$

The contribution to $W_{\rm inc}$ from the $|\Delta m| = 1$ type of processes: $W_{\rm inc}^{|\Delta m|=1}$ is obtained from Eqs. (35) and (36),

$$W_{\rm inc}^{|\Delta m|=1} \equiv (8\pi/3)\int d\omega[W_1(\omega)+W_{-1}(\omega)] = (8\pi/3)(W_1+W_{-1}) = [g_s-(2J_e+1)g_4]\,\gamma\left(\Omega_{eg}^2/4\right) \times\left[\Delta^2+(\gamma/2)^2+g_s\Omega_{eg}^2/2\right]^{-1} . \quad (46)$$

In the limit of weak coupling, Eqs. (45) and (46) become [see Appendix B]

$$W_{\rm inc}^{\Delta m=0} = (2J_e+1)\left(g_4-g_s^2\right)\gamma\left(\Omega_{eg}^2/4\right) \times\left[\Delta^2+(\gamma/2)^2\right]^{-1}+O(S^2) , \quad (47)$$

$$W_{\rm inc}^{|\Delta m|=1} = [g_s - (2J_e+1)g_4]\,\gamma\,(\Omega_{eg}^2/4) \times \left[\Delta^2 + (\gamma/2)^2\right]^{-1} + O(S^2)\,. \quad (48)$$

We now recognize that $W_{\rm inc}^{|\Delta m|=1}$ (in the limit $S \to 0$) is precisely the total rate of spontaneous Raman scatterings (summed over photon polarizations and integrated over angle). It could have been obtained by averaging the spontaneous Raman scattering rate out of $|J_g m\rangle$, which can be easily derived using conventional wave function perturbation theory,

$$r_m = \gamma[1-(2J_e+1)f_m^2](f_m\Omega_{eg}/2)^2[\Delta^2+(\gamma/2)^2]^{-1}\,, \quad (49)$$

over the ground-state population which is given in the limit of weak coupling by w_m [26]. The interpretation of $W_{\rm inc}^{\Delta m=0}$ is also straightforward. It is simply the incoherent part of the Rayleigh scattering. The perturbative rate for the Rayleigh scattering out of $|J_g m\rangle$ is given by

$$R_m = \gamma(2J_e+1)f_m^2(f_m\Omega_{eg}/2)^2[\Delta^2+(\gamma/2)^2]^{-1}\,. \quad (50)$$

The first term in Eq. (47) is simply the average of this rate over the ground-state population w_m. The second term corresponds to the coherent Rayleigh scattering [see Eq. (42)], and is substracted out of the total rate of Rayleigh scattering to give us the incoherent part.

We have thus come to the conclusion that in the limit of weak coupling ($S \to 0$), the incoherent part of the resonance fluorescence spectrum of a Zeeman-degenerate transition ($J_g \neq 0$) is completely accounted for by the spontaneous Raman scattering and the incoherent Rayleigh scattering. The spontaneous Raman scattering accounts for the $|\Delta m| = 1$ type of processes. And the incoherent Rayleigh scattering accounts for the $\Delta m = 0$ type of processes. Since both the spontaneous Raman scattering and the incoherent Rayeigh scattering are processes among ground-state Zeeman sublevels which involve only a single pump photon and a single spontaneous photon, they show up as narrow structures for weak laser-atom couplings. The widths of these structures are induced by the laser field itself and can theoretically be infinitely small [see Appendix C]. The presence of such narrow structures in the resonance fluorescence spectrum is not entirely new. Polder and Schuurmans found it a long time ago in their results for a $J_g = 1/2$ to $J_e = 1/2$ transition [22].

In terms of the relative importance of the incoherent Rayleigh scattering, transitions with $\Delta J = 0$ and those with $\Delta J = 1$ [25] are again very different. Defining

$$q_0(J_g, J_e) \equiv \frac{(2J_e+1)(g_4 - g_s^2)}{g_s - (2J_e+1)g_s^2}\,. \quad (51)$$

We have from Eqs. (43) and (45):

$$W_{\rm inc}^{\Delta m=0}/W_{\rm inc} = q_0(J_g, J_e) + O(S)\,. \quad (52)$$

The parameter $q_0(J_g, J_e)$, therefore, characterizes the relative contribution of the incoherent Rayleigh scattering

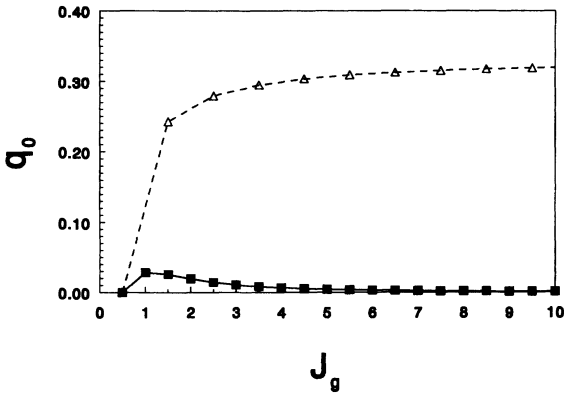

FIG. 4. $q_0(J_g, J_e)$ vs J_g. Solid squares are for $\Delta J = 1$ type of transitions. Triangles are for $\Delta J = 0$ type of transitions. Lines are drawn to guide the eyes.

to the incoherent part of the spectrum in the limit of weak coupling. Some values of this parameter are given in Table I. More data are gathered in Fig. 4. For $\Delta J = 1$ type of transitions, the incoherent Rayleigh scattering is rather insignificant. The maximum value of q_0, achieved by a $J_g = 1$ to $J_e = 2$ transition, is less than 3%. For $\Delta J = 0$ type of transitions, on the other hand, the incoherent Rayleigh scattering contributes significantly to the spectrum for virtually all transitions, with the $J_g = 1/2$ to $J_e = 1/2$ transition being the only exception.

Notice that the factor $g_4 - g_s^2$, which appears in Eqs. (45), (47), and (51) can also be written as

$$g_4 - g_s^2 = \sum_{m=-J_g}^{J_g} w_m \left(f_m^2 - g_s\right)^2 \geq 0\,.$$

It describes the deviation of f_m^2 from its averaged value g_s [Eq. (17)]. If $|f_m|$ is independent of m, $g_4 - g_s^2$ is zero and there would be no incoherent Rayleigh scattering (transitions with $J_g = 0$ and $1/2$ are the examples). It is, therefore, the fact that different m states can couple to the laser field differently, that gives rise to the incoherent Rayleigh scattering. It should be emphasized that

TABLE I. Values for $p_{\rm inc}(J_g, J_e)$ and $q_0(J_g, J_e)$.

J_g	J_e	$p_{\rm inc}(J_g, J_e)$	$q_0(J_g, J_e)$
0	1	0	
1/2	3/2	0.333333	0
1	2	0.411765	0.0285714
3/2	5/2	0.44	0.025974
2	3	0.453362	0.0196704
5/2	7/2	0.461224	0.0144811
3	4	0.466584	0.0108133
7/2	9/2	0.470566	0.00828744
4	5	0.473679	0.006524
1/2	1/2	0.666667	0
3/2	3/2	0.88	0.242424
5/2	5/2	0.925538	0.279698
7/2	7/2	0.945804	0.295132

neither the coherent nor the incoherent Rayleigh scattering can be attributed to individual m states separately, i.e., they cannot be written as sums of contributions from each m state, even though we can do so for the total rate of Rayleigh scattering. All m states participate in deciding how much Rayleigh scattering is scattered coherently and how much is scattered incoherently.

III. RESULTS AND DISCUSSIONS

For the set of parameters used in Fig. 1, the saturation parameter S is 10^{-4}, which put us in the region of the weak coupling (see Appendix B). With the discussions in Sec. II B, the interpretation of Fig. 1 is now straightforward. The little bump at $\omega = \omega_L$ is the incoherent Rayleigh resonance. It is small because the incoherent Rayleigh scattering is insignificant for $\Delta J = 1$ type of transitions. The rest of the resonances in Fig. 1 are spontaneous Raman resonances. This interpretation becomes more transparent by showing $W_{0,\mathrm{inc}}(\omega)$ and $W_1(\omega)$ separately as in Fig. 5. From Sec. II B, we already know that in the limit of weak coupling, $W_{0,\mathrm{inc}}(\omega)$ is due to the incoherent Rayleigh scattering and $W_1(\omega)$ is due to the spontaneous Raman scattering. We will come back to this example momentarily to discuss its other features.

More results are presented in this section. All of them are calculated by a single program which applies to arbitrary angular momentum, detuning, and Rabi frequency. The spectra shown will be $W_{0,\mathrm{inc}}(\omega)$ and $W_1(\omega)$ $[W_{-1}(\omega) = W_1(\omega)]$, since they are in fact more closely related to experimental measurements through Eqs. (11)–(13), and they can be determined separately. Other spectra are related to $W_{0,inc}(\omega)$ and $W_1(\omega)$ through Eqs. (20)–(30).

A. Weak coupling

In the limit of weak coupling, $W_{0,\mathrm{inc}}(\omega)$ comes from the incoherent Rayleigh scattering, and $W_1(\omega)$ comes from the spontaneous Raman scattering. As pointed out in Sec. II B, transitions with $J_g = 1/2$ ($J_e = 1/2$ or $3/2$) do not have the incoherent Rayleigh resonance. This is illustrated in Fig. 6 (see also Fig. 9) for a $J_g = 1/2$ to $J_e = 3/2$ transition with $\Delta = -0.5\gamma$ and $S = 0.01$ ($\Omega_{eg} = 0.244949\gamma$). We also pointed out that the contribution of the incoherent Rayleigh scattering is very significant for all $\Delta J = 0$ type of transitions with the exception of the $J_g = 1/2$ to $J_e = 1/2$ transition. Figure 7 illustrates this point using a $J_g = 5/2$ to $J_e = 5/2$ transition with $\Delta = -0.5\gamma$ and $S = 0.01$ ($\Omega_{eg} = 0.897651\gamma$).

One might have noticed in Fig. 1 that spontaneous Raman resonances are roughly equally spaced. This turns out to be a general characteristic of the weak-coupling spectra in the limit of large detuning where spontaneous Raman resonances are well separated. For a transition with ground-state angular momentum J_g, there are $2J_g$ spontaneous Raman resonances in $W_1(\omega)$. We show in Appendix C that these resonances become well separated for sufficiently large detunings (compare, for example, Fig. 8 with Fig. 7), and in which case $W_1(\omega)$ can be represented by a simple analytic formula

$$W_1(\omega) = (3/8\pi) \sum_{m=-J_g+1}^{J_g} w_m u_m \times \left\{ \frac{1}{\pi} \frac{\eta_m}{[(\omega - \omega_L) - \delta_m]^2 + \eta_m^2} \right\}, \quad (53)$$

where the frequency shift δ_m and the (half) width η_m are given by Eqs. (C7) and (C8), respectively, and where

$$u_m = (2J_e + 1)\gamma h_m^2 (f_m \Omega_{eg}/2)^2 [\Delta^2 + (\gamma/2)^2]^{-1}, \quad (54)$$

is precisely the perturbative spontaneous Raman scattering rate from $m_g = m$ to $m_g = m - 1$ (summed over photon polarizations and integrated over angle). The wave function perturbation theory is, therefore, not only able to predict the integrated rates over all frequencies, but is also able to predict the integrated rates over *individual* resonances when they are well separated. (u_m differs from r_m [Eq. (49)] in that r_m includes also the sponta-

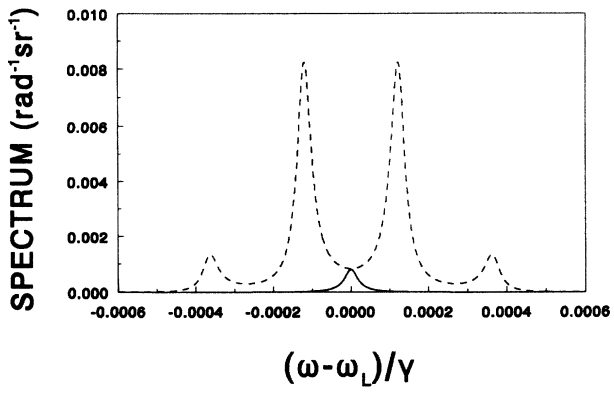

FIG. 5. The same as Fig. 1 except what is shown are $W_{0,\mathrm{inc}}(\omega)$ (solid line), and $W_1(\omega)$ (dash line).

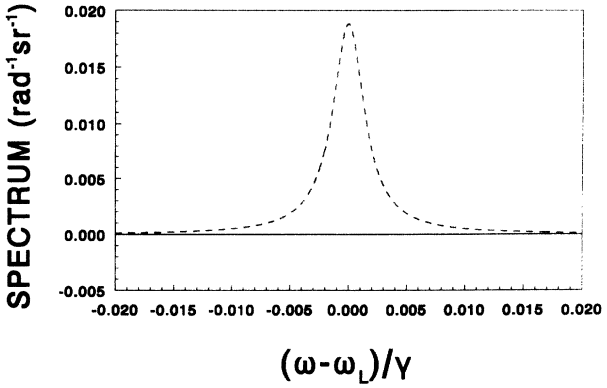

FIG. 6. The spectrum for a $J_g = 1/2$ to $J_e = 3/2$ transition with $\Delta = -0.5\gamma$ and $S = 0.01$. Solid line: $W_{0,\mathrm{inc}}(\omega)$. Dash line: $W_1(\omega)$.

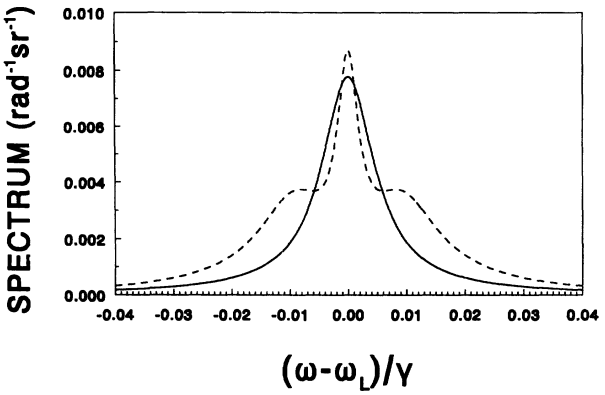

FIG. 7. The spectrum for a $J_g = 5/2$ to $J_e = 5/2$ transition with $\Delta = -0.5\gamma$ and $S = 0.01$. Solid line: $W_{0,\mathrm{inc}}(\omega)$. Dash line: $W_1(\omega)$.

neous Raman scattering from $m_g = m$ to $m_g = m + 1$).

By using the explicit expressions for f_m [30],

$$f_m = \begin{cases} 2^{1/2}[(J_g+1)^2 - m^2][(2J_g+3)(2J_g+2) \\ \quad \times(2J_g+1)]^{-1/2} \quad \text{for } J_e = J_g + 1 \ , \\ 2m[(2J_g+2)(2J_g+1)(2J_g)]^{-1/2} \quad \text{for } J_e = J_g \ , \end{cases} \tag{55}$$

the frequency shifts δ_m [Eq. (C7)] can be written as

$$\delta_m = \begin{cases} -(2m-1)g_s^{-1}[(2J_g+3)(2J_g+2) \\ \quad \times(2J_g+1)]^{-1} S\Delta \quad \text{for } J_e = J_g + 1 \\ 2(2m-1)g_s^{-1}[(2J_g+2)(2J_g+1)(2J_g)]^{-1} S\Delta \\ \quad \text{for } J_e = J_g \ . \end{cases} \tag{56}$$

The spontaneous Raman resonances are, therefore, equally spaced for both $\Delta J = 0$ and $\Delta J = 1$ types of transitions, with spacings given by

$$v = \begin{cases} 2g_s^{-1}[(2J_g+3)(2J_g+2)(2J_g+1)]^{-1} S|\Delta| \\ \quad \text{for } J_e = J_g + 1 \\ 4g_s^{-1}[(2J_g+2)(2J_g+1)(2J_g)]^{-1} S|\Delta| \\ \quad \text{for } J_e = J_g \ . \end{cases} \tag{57}$$

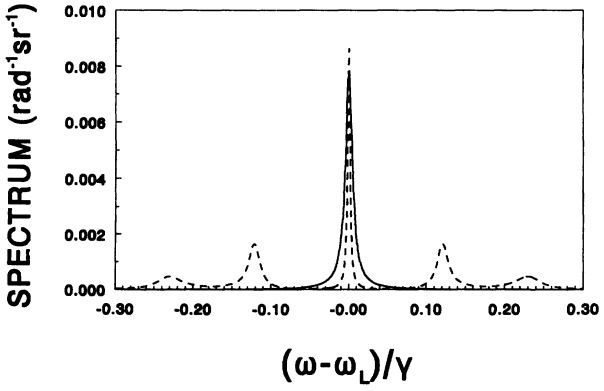

FIG. 8. The same as Fig. 7 except that $\Delta = -8\gamma$.

For the set of parameters in Fig. 1, v works out to be $2.44 \times 10^{-4}\gamma$. For Fig. 8, we obtain a spacing of 0.12γ. It should be emphasized that except for transitions with $J_g = 1/2$ ($J_e = 1/2$ or $3/2$), Eq. (53) is valid only when the detuning is sufficiently large that all $2J_g$ spontaneous Raman resonances are well separated. It fails for small detunings where spontaneous Raman resonances overlap and interact with each other, as is the case in Fig. 7. Transitions with $J_g = 1/2$ are special because they have only a single spontaneous Raman resonance. Equation (53), which reduces for $J_g = 1/2$ to a single term corresponding to $m = 1/2$, is then valid regardless of detuning.

The most important characteristic of weak-coupling spectra may be their scaling. From Appendix B, we already know that the integrated rates scaled by γ depend only on the saturation parameter S. This brings us naturally to the question of which parameters determine the shape of the spectrum. Just like the case for integrated rates, the set of parameters Δ/γ and Ω_{eg}/γ (or S) may be overcomplete. In the limit of weak coupling, it can be shown from Eqs. (8), (9), (A13)–(A16), (A19), (A24), and (C1)–(C4) that other than a frequency-scaling factor $S\gamma$, $W_{0,\mathrm{inc}}(\omega)$ is determined solely by geometry (f_ms and h_ms), and $W_1(\omega)$ is determined, in addition to geometry, by Δ/γ only. The validity of this statement does *not* require that the spontaneous Raman resonances to be well separated. Figures 9–14 show, for different transitions, some of the weak-coupling spectra with frequency scaled by $S\gamma$. We will call them the generic weak-coupling spectra (GWCS). For $W_1(\omega)$, the corresponding GWCS depends generally on both Δ/γ and geometry. But for fixed Δ/γ, it is valid for arbitrary S satisfying $S \ll 1$. For $W_{0,\mathrm{inc}}(\omega)$, the corresponding GWCS is not only independent of S, but also independent of Δ/γ. It is determined solely by geometry (f_ms and h_ms) as long as $S \ll S_0$ is satisfied (S_0 is defined in Appendix B). In reading Figs. 9–14, particular attention should be paid to the differences between the $\Delta J = 0$ and $\Delta J = 1$ types

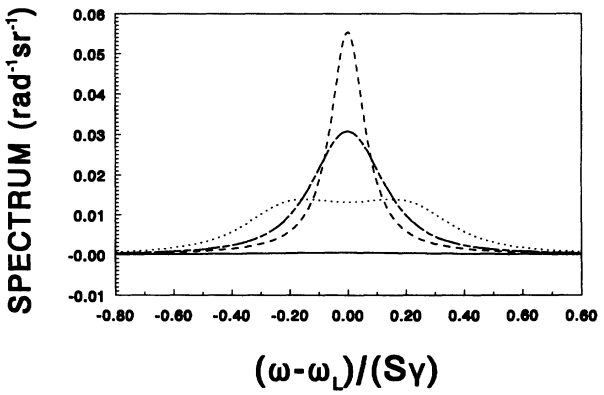

FIG. 9. The generic weak-coupling spectra for a $J_g = 1$ to $J_e = 2$ transition. Solid line: the generic $W_{0,\mathrm{inc}}$, which is valid for all (Δ/γ)s and (Ω_{eg}/γ)s satisfying $S \ll S_0 = 2.04 \times 10^{-2}$. Dash line, dash-dotted line, and dotted line: the generic W_1s for $|\Delta|/\gamma = 0, 1, 2$, respectively. They are valid for all (Ω_{eg}/γ)s satisfying $S \ll 1$.

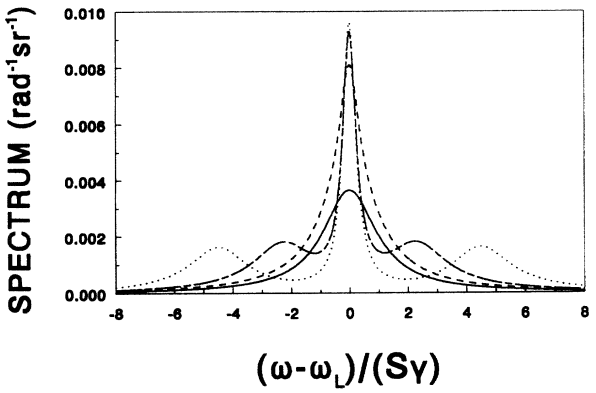

FIG. 10. The same as Fig. 9 except that it is for $J_g = 3/2$ to $J_e = 3/2$ transition with $S_0 = 2.29$.

of transitions. For the $\Delta J = 1$ type of transitions, the incoherent Rayleigh resonances (in $W_{0,\mathrm{inc}}$) are not even visible. They are so small that they can only been seen on a much smaller y scale (see, e.g., Fig. 5). Figure 14 shows the generic $W_{0,\mathrm{inc}}$ for a 4 to 5 transition on a much smaller y scale, along with the generic W_1 for $|\Delta|/\gamma = 20$. For $\Delta J = 0$ type of transitions, on the other hand, the incoherent Rayleigh scattering is very significant, as can be seen in Figs. 10 and 12.

Even though the GWCS for $W_1(\omega)$ does depend on Δ/γ, this dependence is rather trivial in the limit of well-separated resonances, in which case $W_1(\omega)$ is given by Eq. (53), and the corresponding GWCS is easily recognized by rewriting it as

$$W_1(\omega) = (3/8\pi) \sum_{m=-J_g+1}^{J_g} w_m \bar{u}_m \times \left\{ \frac{1}{\pi} \frac{\bar{\eta}_m}{[(\omega-\omega_L)/(S\gamma) - \bar{\delta}_m]^2 + \bar{\eta}_m^2} \right\}, \quad (58)$$

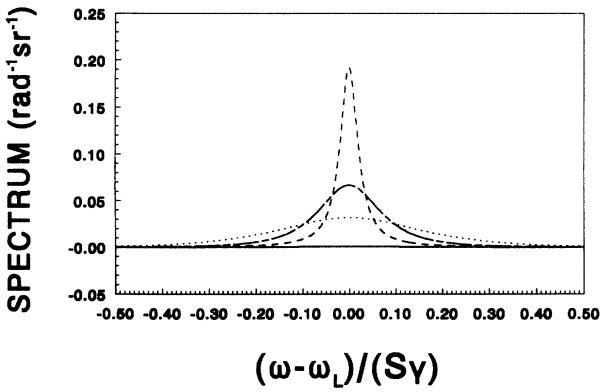

FIG. 11. The same as Fig. 9 except that it is for $J_g = 2$ to $J_e = 3$ transition with $S_0 = 1.66 \times 10^{-2}$. See Fig. 5 for the shape of the spectrum at a much larger detuning. Simply rescaling the x axis in Fig. 5 by $S = 1 \times 10^{-4}$ gives us the GWCS at $|\Delta|/\gamma = 20$. Notice that the y scales in two figures are very different.

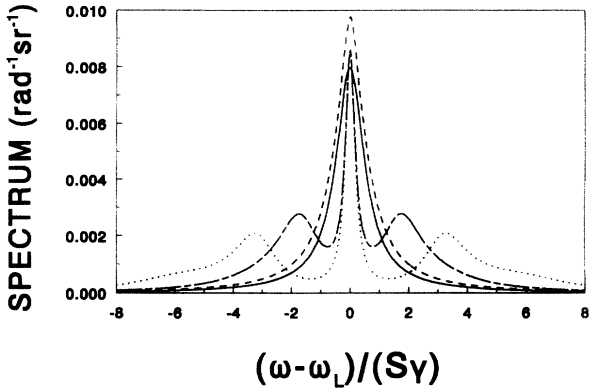

FIG. 12. The same as Fig. 9 except that it is for $J_g = 5/2$ to $J_e = 5/2$ transition with $S_0 = 1.4$. See Figs. 7 and 8 for the shape of the spectrum at larger detunings.

where

$$\bar{u}_m = (2g_s)^{-1}(2J_e+1) f_m^2 h_m^2 \quad (59)$$

$$\bar{\delta}_m = (2g_s)^{-1}(f_m^2 - f_{m-1}^2)(\Delta/\gamma) \quad (60)$$

$$\bar{\eta}_m = (4g_s)^{-1} \Big\{ f_m^2[1-(2J_e+1)f_m^2] + f_{m-1}^2[1-(2J_e+1)f_{m-1}^2] + (2J_e+1)(f_m^2 - f_{m-1}^2)^2 \Big\}. \quad (61)$$

Obviously, after rescaling $\omega - \omega_L$ by $S\gamma$, the resulting GWCS depends only on (Δ/γ) and geometric factors. As long as we remain in the region of well-separated resonances, changing Δ/γ affects only the positions of the resonances in the GWCS. The shapes (both the widths and the heights) of individual resonances are not affected and are determined solely by geometry (f_ms and h_ms).

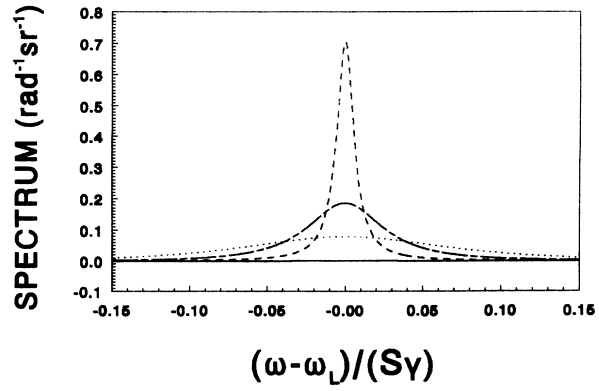

FIG. 13. The same as Fig. 9 except that it is for $J_g = 4$ to $J_e = 5$ transition with $S_0 = 5.91 \times 10^{-3}$.

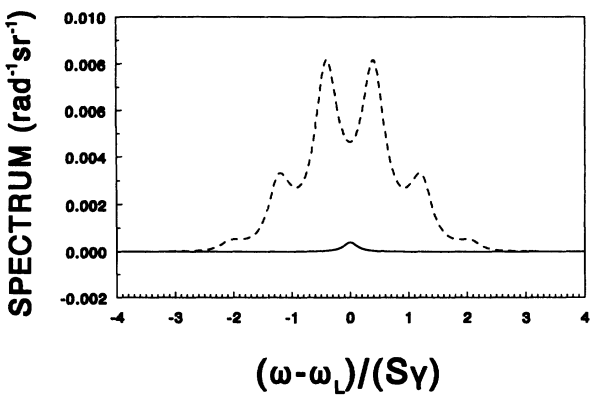

FIG. 14. The generic weak-coupling spectrum for a $J_g = 4$ to $J_e = 5$ transition on a small y scale. Solid line: the generic $W_{0,\mathrm{inc}}$, valid for all (Δ/γ)s and (Ω_{eg}/γ)s satisfying $S \ll S_0 = 5.91 \times 10^{-3}$. Dash line: the generic W_1 for $|\Delta|/\gamma = 20$, valid for all (Ω_{eg}/γ)s satisfying $S \ll 1$.

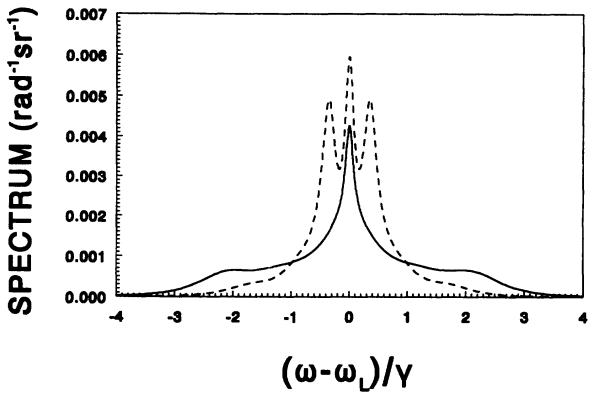

FIG. 16. The spectrum for a $J_g = 5/2$ to $J_e = 5/2$ transition with $|\Delta|/\gamma = 0.5$ and $S = 0.5$ ($\Omega_{eg}/\gamma = 6.34735$). Solid line: $W_{0,\mathrm{inc}}(\omega)$. Dash line: $W_1(\omega)$.

B. Intermediate and strong couplings

As laser-atom coupling gets stronger (i.e., S gets bigger), broad structures with the width of the order of γ start to develop. This is shown in Fig. 15 for a $J_g = 2$ to $J_e = 3$ transition at $S = 0.5$. These broad structures come from processes that involve multiple pump and multiple spontaneous photons [31], corresponding to the S^2 and high order terms in the S expansions of the integrated rates (Appendix B). With the arrival of these broad structures, the dependence of the line shape on the saturation parameter S is no longer through a simple scaling factor, as can be seen by comparing Fig. 16 with Fig. 7. Figure 17 is another intermediate-coupling spectrum for a $J_g = 3/2$ to $J_e = 3/2$ transition with $|\Delta|/\gamma = 3$ and $S = 1$. Figures 18–20 represent some typical strong-coupling spectra. Figure 18 is the spectrum for a $J_g = 1$ to $J_e = 2$ transition with $|\Delta|/\gamma = 2$ and $S = 30$. Figure 19 is the spectrum for a $J_g = 2$ to $J_e = 3$ transition with $|\Delta|/\gamma = 2$ and $S = 30$. Figure 20 is the spectrum for a $J_g = 3/2$ to $J_e = 3/2$ transition with $|\Delta|/\gamma = 3$ and $S = 10$. The qualitative features of all these spectra, including both the intermediate-coupling spectra and the strong-coupling spectra, can be best understood using the dressed-state picture [31]. For a transition with a ground-state angular momentum J_g, there are $2J_g + 1$ dressed-state manifolds, one for each m_g. Each manifold is coupled to its neighbors, $|\Delta m| = 1$, by the spontaneous decay. $W_0(\omega)$ is the result of intramanifold, i.e., $|\Delta m| = 0$, processes. It is, therefore, made up of $2J_g + 1$ Mollow triplets. The center peak of these triplets always overlap, and because of the degeneracy between $m_g = m$ and $m_g = -m$ manifolds in the absence of any magnetic field, the side bands of $W_0(\omega)$ can have at most $J_g + 1$ peaks for integer J_gs and $J_g + 1/2$ peaks for half integer J_gs. Of course, the peaks in the two side bands may not be resolved depending on the values of Δ/γ and S. $W_1(\omega)$ is the result of intermanifold, i.e., $\Delta m = -1$, processes. For an atom in a linearly polarized laser field, the Rabi splitting of a dressed-state manifold depends on $|m_g|$, i.e., it is different for manifolds with different $|m_g|$. It is then easy to see that $W_1(\omega)$ is made up of J_g

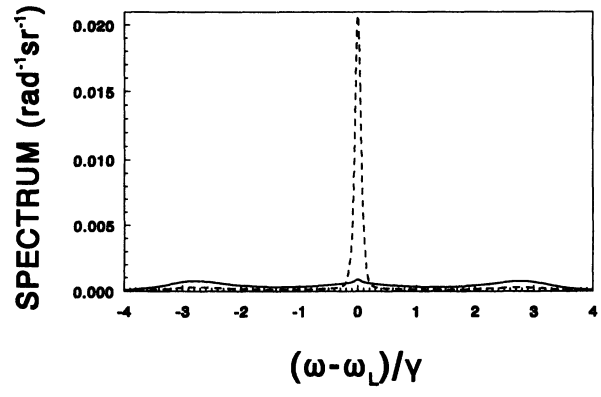

FIG. 15. The spectrum for a $J_g = 2$ to $J_e = 3$ transition with $|\Delta|/\gamma = 2$ and $S = 0.5$ ($\Omega_{eg}/\gamma = 7.37724$). Solid line: $W_{0,\mathrm{inc}}(\omega)$. Dash line: $W_1(\omega)$.

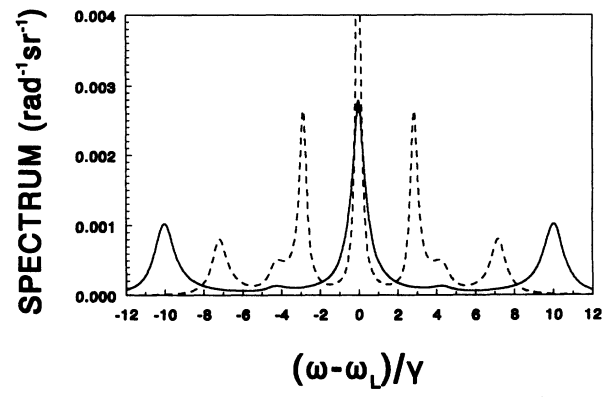

FIG. 17. The spectrum for a $J_g = 3/2$ to $J_e = 3/2$ transition with $|\Delta|/\gamma = 3$ and $S = 1$ ($\Omega_{eg}/\gamma = 24.8328$). Solid line: $W_{0,\mathrm{inc}}(\omega)$. Dash line: $W_1(\omega)$.

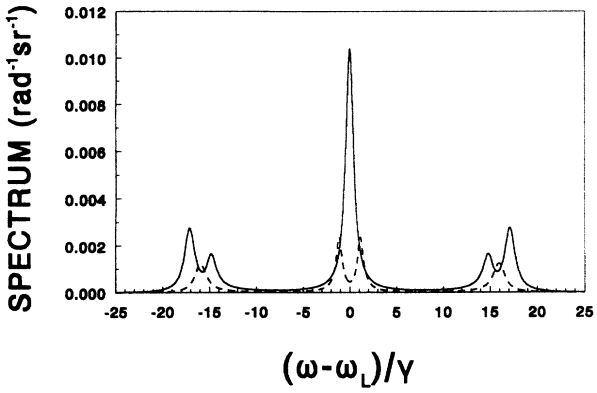

FIG. 18. The spectrum for a $J_g = 1$ to $J_e = 2$ transition with $|\Delta|/\gamma = 2$ and $S = 30$ ($\Omega_{eg}/\gamma = 46.5564$). Solid line: $W_{0,\mathrm{inc}}(\omega)$. Dash line: $W_1(\omega)$.

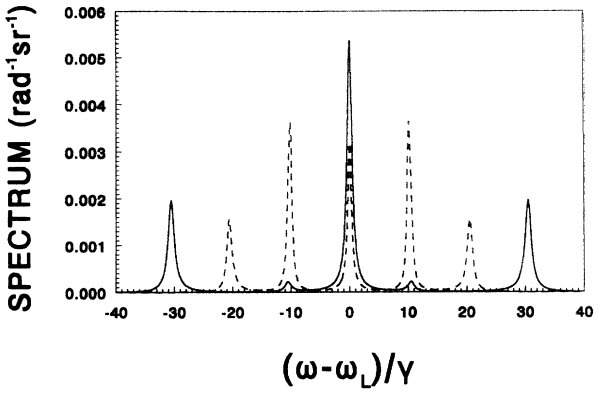

FIG. 20. The spectrum for a $J_g = 3/2$ to $J_e = 3/2$ transition with $|\Delta|/\gamma = 3$ and $S = 10$ ($\Omega_{eg}/\gamma = 78.5281$). Solid line: $W_{0,\mathrm{inc}}(\omega)$. Dash line: $W_1(\omega)$.

quadruplets for integer J_g and of $J_g - 1/2$ quadruplets and 1 triplet for half integer J_g. The one triplet for half integer J_g comes from processes from manifold $m = 1/2$ to manifold $m = -1/2$, both of which have the same Rabi splitting. Again, depending on the specific values of Δ/γ and S, we may not be able to resolve all the resonances.

The spectra for $\Delta J = 0$ and $\Delta J = 1$ types of transitions look very different in the limit of large S (compare for example Figs. 19 and 20). This difference comes from the different behavior of f_m as given by Eq. (55). In the limit of large S, the Rabi splitting for the $m_g = m$ manifold is given by

$$|f_m \Omega_{eg}| ,$$

from which and Eq. (55) it is easy to show for example that for $\Delta J = 0$ type of transitions [25] the spacing between resonances is a multiple of

$$[(2J_g + 2)(2J_g + 1)(2J_g)]^{-1/2}|\Omega_{eg}| , \qquad (62)$$

in the limit of large S. With the parameters used in Fig. 20, this turns out to be 10.14γ. The positioning of resonances for $\Delta J = 1$ type of transitions can be understood in a similar fashion.

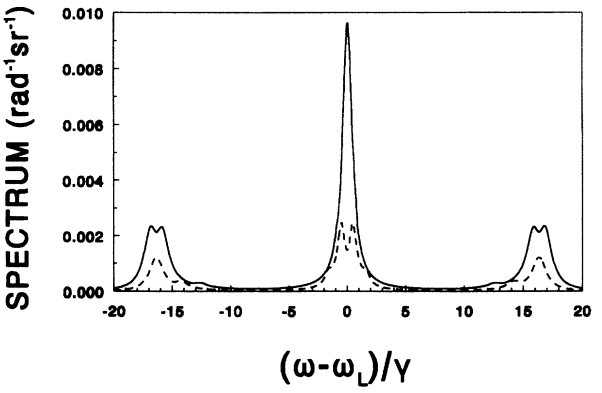

FIG. 19. The spectrum for a $J_g = 2$ to $J_e = 3$ transition with $|\Delta|/\gamma = 2$ and $S = 30$ ($\Omega_{eg}/\gamma = 57.1438$). Solid line: $W_{0,\mathrm{inc}}(\omega)$. Dash line: $W_1(\omega)$.

C. The cycling transition of Cs

It is a rather simple matter to put our spectra on an absolute frequency scale. All we need to calculate is basically the reduced dipole matrix element, since the frequency of a transition is usually known. For transitions between hyperfine levels, the reduced dipole matrix element can be obtained using [32]

$$\langle (J'I)F'||\mu||(JI)F\rangle = (-1)^{J'+I+F+1}[(2F'+1)(2F+1)]^{1/2} \begin{Bmatrix} F' & 1 & F \\ J & I & J' \end{Bmatrix} \langle J'||\mu||J\rangle . \qquad (63)$$

For the cycling transition of cesium, we have then

$$\langle (6p_{3/2}I = 7/2)F_e = 5||\mu||(6s_{1/2}I = 7/2)F_g = 4\rangle = \frac{1}{2}\sqrt{11}\langle 6p_{3/2}||\mu||6s_{1/2}\rangle , \qquad (64)$$

where the value of $\langle 6p_{3/2}||\mu||6s_{1/2}\rangle$ can be taken either from theory [33] or from experiment [34]. Using the experimental result of $\langle 6p_{3/2}||\mu||6s_{1/2}\rangle = 6.36$ a.u., we obtain

$$\langle (6p_{3/2}I = 7/2)F_e = 5||\mu||(6s_{1/2}I = 7/2)F_g = 4\rangle = 10.55 \text{ a.u.}$$

Substituting it into Eq. (5) and using $\lambda_{eg} = 852$ nm, we arrive at $\gamma = 5.28$ MHz. The reduced Rabi frequency can be calculated from the electric field using Eq. (6), which can also be written as

$$\Omega_{eg}/(2\pi) = (I_L/I_a)^{1/2}[\langle F_e||\mu||F_g\rangle \text{ (a.u.)}] \times 6.579 \times 10^{15} \text{ Hz} , \qquad (65)$$

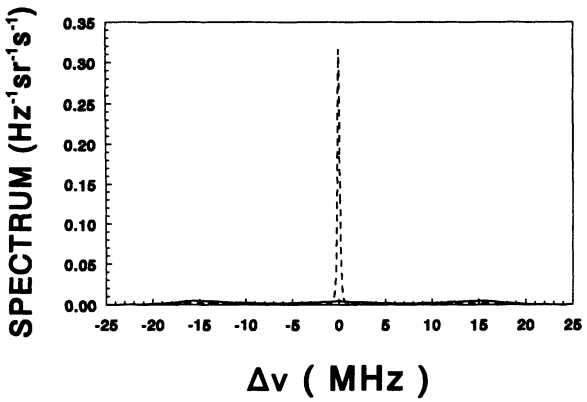

FIG. 21. The spectrum for the cycling transition of Cs [$F_g = 4$, $F_e = 5$, and $\gamma/(2\pi) = 5.28$ MHz] with $|\Delta|/(2\pi) = 10.6$ MHz and $\Omega_{eg}/(2\pi) = 52.4$ MHz (S=0.552 585). Solid line: $W_{0,\mathrm{inc}}(\nu) \equiv 2\pi W_{0,\mathrm{inc}}(\omega)$. Dash line: $W_1(\nu) \equiv 2\pi W_1(\omega)$.

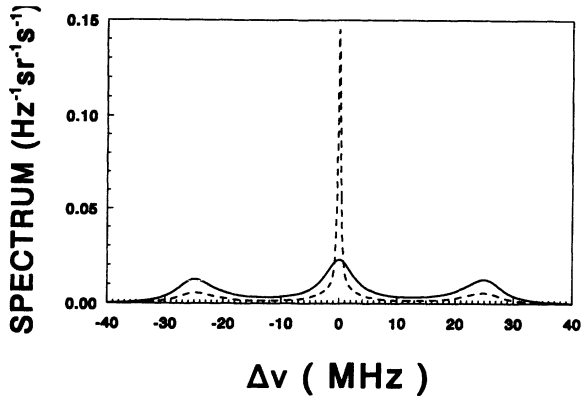

FIG. 22. The same as Fig. 21 except $\Omega_{eg}/(2\pi) = 104.8$ MHz (S=2.201 93).

where I_L refers to the laser intensity, and $I_a = 3.509 \times 10^{16}$ W/cm^2 is the atomic unit of intensity.

In the experiment of Ref. [13], $\Delta/(2\pi) = -10.6$ MHz and $I_L = 20$ mW/cm^2, corresponding to 10 mW/cm^2 for each of the two counterpropagating σ^+ and σ^- beams. In this case $\Omega_{eg}/(2\pi) = 52.4$ MHz and $S = 0.552\,585$. The spectra $W_{0,\mathrm{inc}}(\nu) \equiv 2\pi W_{0,inc}(\omega)$ and $W_1(\nu) \equiv 2\pi W_1(\omega)$ for this set of parameters are shown in Fig. 21. Figure 22 is the spectrum for the same detuning but with $\Omega_{eg}/(2\pi) = 104.8$ MHz ($S = 2.201\,93$), corresponding to $I_L = 80$ mW/cm^2.

IV. CONCLUSIONS

The resonance fluorescence spectrum for a closed two-level Zeeman-degenerate atom interacting with a linearly polarized coherent laser field has been discussed in some detail. The major surprises to me have been the incoherent Rayleigh resonance and the role of the incoherent Rayleigh scattering in determining the widths of the spontaneous Raman resonances (Appendix C). My expectation had been that the incoherent scattering in the limit of weak coupling would come solely from spontaneous Raman processes. This turns out to be only roughly correct for $\Delta J = 1$ type of transitions and very wrong for all $\Delta J = 0$ type of transitions with the exception of the $J_g = 1/2$ to $J_e = 1/2$ transition.

Finally, I stress that effects of the atomic motion have not been considered in this publication. Complexities due to these effects arise not only in cases where the atomic motion has to be treated quantum mechanically [10,14,16,18]. Even in the traditional Doppler broadening region, subtleties raised recently by Wilkens [35] and Baxter *et al.* [36] need to be better addressed.

ACKNOWLEDGMENTS

I would like to thank Jinx Cooper for helpful discussions.

APPENDIX A: CALCULATING THE RESOLVENT OPERATOR

This appendix provides more details on how to calculate the resolvent operator. We assume that readers are familar with the Liouville space representation [37–39].

For a transition with ground-state angular momentum J_g and excited-state angular momentum J_e, the Liouville space has a dimension of $[2(J_e + J_g + 1)]^2$. The calculation of the resolvent operator $R(s) = [\mathcal{L}(s)]^{-1}$ generally requires the inversion of a $[2(J_e+J_g+1)]^2 \times [2(J_e+J_g+1)]^2$ matrix. But as pointed out in paper I, the representation of the operator $\mathcal{L}(s) \equiv s - L_A^R$ in the Liouville space $|J_1 m_1, J_2 m_2\rangle\rangle$ is block diagonal in $l \equiv m_1 - m_2$ because of the cylindrical symmetry. All nonzero matrix elements of L_A^R [defined by Eq. (2)] are given by

$$\langle\langle J_e m', J_g m' - l' | L_A^R | J_e m, J_g m - l\rangle\rangle = (-\gamma/2 + i\Delta)\delta_{m'm}\delta_{l'l} , \tag{A1}$$

$$\langle\langle J_g m', J_e m' - l' | L_A^R | J_g m, J_e m - l\rangle\rangle = (-\gamma/2 - i\Delta)\delta_{m'm}\delta_{l'l} , \tag{A2}$$

$$\langle\langle J_e m', J_e m' - l' | L_A^R | J_e m, J_e m - l\rangle\rangle = -\gamma\delta_{m'm}\delta_{l'l} , \tag{A3}$$

$$\begin{aligned}\langle\langle J_g m', J_g m' - l' | L_A^R | J_e m, J_g m - l\rangle\rangle &= \langle\langle J_e m', J_g m' - l' | L_A^R | J_g m, J_g m - l\rangle\rangle \\ &= \langle\langle J_g m', J_e m' - l' | L_A^R | J_e m, J_e m - l\rangle\rangle \\ &= \langle\langle J_e m', J_e m' - l' | L_A^R | J_g m, J_e m - l\rangle\rangle \\ &= i(\Omega_{eg}/2) f_m \delta_{m'm}\delta_{l'l} ,\end{aligned} \tag{A4}$$

$$\begin{aligned}\langle\langle J_g m', J_g m' - l'|L_A^R|J_g m, J_e m - l\rangle\rangle &= \langle\langle J_e m', J_g m' - l'|L_A^R|J_e m, J_e m - l\rangle\rangle \\ &= \langle\langle J_g m', J_e m' - l'|L_A^R|J_g m, J_g m - l\rangle\rangle \\ &= \langle\langle J_e m', J_e m' - l'|L_A^R|J_e m, J_g m - l\rangle\rangle \\ &= -i(\Omega_{eg}/2) f_m \delta_{m'm}\delta_{l'l} \ , \end{aligned} \tag{A5}$$

$$\langle\langle J_g m', J_g m' - l'|L_A^R|J_e m, J_e m - l\rangle\rangle = \gamma\langle J_g m' 1 m - m'|J_e m\rangle\langle J_g m' - l 1 m - m'|J_e m - l\rangle\delta_{l'l} \ . \tag{A6}$$

We can, therefore, deal with each l manifold separately.

For $J_e = J_g$ type of transtions, there are $4(J_g + 1)$ l manifolds with dimensions $4(2J_g + 1 - |l|)$ ($l = -2J_g, \ldots, 2J_g$). The representation of $\mathcal{L}(s)$ in each l manifold, $\mathcal{L}^{(l)}(s)$, has the same form for all l,

$$\mathcal{L}^{(l)}(s) = \begin{pmatrix} aI & A^{(l)} & B^{(l)} & C^{(l)} \\ A^{(l)} & bI & 0 & B^{(l)} \\ B^{(l)} & 0 & cI & A^{(l)} \\ 0 & B^{(l)} & A^{(l)} & dI \end{pmatrix} . \tag{A7}$$

Here a, b, c, and d are defined by $a = s$, $b = s - i\Delta + \gamma/2$, $c = s + i\Delta + \gamma/2$, and $d = s + \gamma$. I represents a unit matrix of dimension $(2J_g + 1 - |l|)$. $A^{(l)}$, $B^{(l)}$, and $C^{(l)}$ are all matrices of dimension $(2J_g + 1 - |l|)$. Their matrix elements are defined by

$$\langle m'|A^{(l)}|m\rangle \equiv -\langle\langle J_e m', J_g m' - l|L_A^R|J_g m, J_g m - l\rangle\rangle \ , \tag{A8}$$

$$\langle m'|B^{(l)}|m\rangle \equiv -\langle\langle J_g m', J_e m' - l|L_A^R|J_g m, J_g m - l\rangle\rangle \ , \tag{A9}$$

$$\langle m'|C^{(l)}|m\rangle \equiv -\langle\langle J_g m', J_g m' - l|L_A^R|J_e m, J_e m - l\rangle\rangle \ . \tag{A10}$$

It is obvious from Eqs. (A4)–(A6) that both $A^{(l)}$ and $B^{(l)}$ are diagonal matrices, and $C^{(l)}$ is tridiagonal. The corresponding $R^{(l)}(s) = [\mathcal{L}^{(l)}(s)]^{-1}$ can be written as

$$R^{(l)}(s) = \begin{pmatrix} R^{(l)}_{gg,gg} & R^{(l)}_{gg,eg} & R^{(l)}_{gg,ge} & R^{(l)}_{gg,ee} \\ R^{(l)}_{eg,gg} & R^{(l)}_{eg,eg} & R^{(l)}_{eg,ge} & R^{(l)}_{eg,ee} \\ R^{(l)}_{ge,gg} & R^{(l)}_{ge,eg} & R^{(l)}_{ge,ge} & R^{(l)}_{ge,ee} \\ R^{(l)}_{ee,gg} & R^{(l)}_{ee,eg} & R^{(l)}_{ee,ge} & R^{(l)}_{ee,ee} \end{pmatrix} , \tag{A11}$$

where every element is again a matrix of dimension $(2J_g + 1 - |l|)$. It is easy to show that the inversion of the matrix $\mathcal{L}^{(l)}(s)$ can be obtained by inverting a single tridiagonal matrix $Z^{(l)}$ of dimension $(2J_g + 1 - |l|)$,

$$\begin{aligned} Z^{(l)}(s) = \ & (acI + A^{(l)^2} - B^{(l)^2})(bdI + A^{(l)^2} - B^{(l)^2}) \\ & - (a + d)(b + c)A^{(l)^2} + (b + c)C^{(l)}B^{(l)}A^{(l)} \ . \end{aligned} \tag{A12}$$

Defining $Y^{(l)}(s) \equiv [Z^{(l)}(s)]^{-1}$, we have

$$R^{(l)}_{eg,gg}(s) = \left(A^{(l)^2} - B^{(l)^2} - cdI\right) A^{(l)} Y^{(l)}(s) \ , \tag{A13}$$

$$\begin{aligned} R^{(l)}_{eg,eg}(s) = & \left(acI + A^{(l)^2} - B^{(l)^2}\right)^{-1} \left(acdI + aA^{(l)^2}\right. \\ & \left. - dB^{(l)^2} + A^{(l)}C^{(l)}B^{(l)}\right) A^{(l)} Y^{(l)}(s) A^{(l)^{-1}} \\ & \times \left(acI + A^{(l)^2} - B^{(l)^2}\right) , \end{aligned} \tag{A14}$$

$$R^{(l)}_{eg,ge}(s) = -\left[aR^{(l)}_{eg,gg} + R^{(l)}_{eg,eg}(s)A^{(l)}\right] B^{(l)^{-1}} \ , \tag{A15}$$

$$R^{(l)}_{eg,ee}(s) = \left[I - R^{(l)}_{eg,gg}A^{(l)} - bR^{(l)}_{eg,eg}(s)\right] B^{(l)^{-1}} \ , \tag{A16}$$

and so on. Because all matrices other than $Z^{(l)}$ are diagonal, their inversions are trivial.

For $J_e = J_g + 1$ type of transitions, there are $4J_g + 5$ l manifolds. The $l = 0$ manifold has a dimension of $4(2J_g + 1) + 2$. Manifolds $l = \pm 1, \ldots, \pm(2J_g + 1)$ each have $4(2J_g + 2 - |l|)$ dimensions. Two other manifolds, corresponding to $l = \pm(2J_g + 2)$, each have a dimension of 1. The presence of the states $|J_e m_e = -(J_g + 1)\rangle$ and $|J_e m_e = -(J_g + 1)\rangle$ have, therefore, introduced new manifolds and new dimensions into the problem. These changes do not however bring with them much extra work. The matrix elements of $R^{(l)}(s)$ among states $|J_1 m, J_2 m - l\rangle\rangle$ with both $|m| \leq J_g$ and $|m - l| \leq J_g$, which are all we would need for calculating the resonance fluorescence spectrum [Eqs. (8) and (9)], are again given by Eqs. (A13)–(A16), as if states $|J_e m_e = -(J_g + 1)\rangle$ and $|J_e m_e = -(J_g + 1)\rangle$ never existed. This is because in the absence of collisions, the extra dimensions introduced by $|J_e m_e = -(J_g + 1)\rangle$ and $|J_e m_e = -(J_g + 1)\rangle$ are effectively decoupled from other dimensions, in the sense that the inversion of the matrix

$$\begin{pmatrix} X & Z \\ 0 & Y \end{pmatrix}$$

is given by

$$\begin{pmatrix} X^{-1} & -X^{-1}ZY^{-1} \\ 0 & Y^{-1} \end{pmatrix} .$$

[X would correspond to the right-hand side of Eq. (A7).

Y would correspond the extra dimensions.]

Equations (A13)–(A16) are all that is needed to calculate the resonance fluorescence spectrum. For the probe spectrum of a $J_e = J_g + 1$ type of transition [21], we need also $\langle\langle J_eJ_e, J_gJ_g|R^{(1)}(s)|J_eJ_e, J_gJ_g\rangle\rangle$ and $\langle\langle J_eJ_e, J_gJ_g|R^{(1)}(s)|J_eJ_e, J_eJ_g\rangle\rangle$. (Using the terminology introduced earlier, these matrix elements belong to what we called the extra manifolds for $J_g = 0$, and belong to the extra dimensions in $l = 1$ manifold for $J_g \neq 0$.) They can be found by simply inverting a two by two matrix,

$$\begin{pmatrix} s+\gamma/2-i\Delta & if_{J_g}\Omega_{eg}/2 \\ if_{J_g}\Omega_{eg}/2 & s+\gamma \end{pmatrix},$$

because states $|J_eJ_e, J_gJ_g\rangle\rangle$ and $|J_eJ_e, J_eJ_g\rangle\rangle$ are effectively only coupled among themselves [Eqs. (A1)–(A6)]. We obtain

$$\langle\langle J_eJ_e, J_gJ_g|R^{(1)}(s)|J_eJ_e, J_gJ_g\rangle\rangle = (s+\gamma)\left[(s+\gamma)(s+\gamma/2-i\Delta)+(f_{J_g}\Omega_{eg}/2)^2\right]^{-1} \quad \text{(A17)}$$

$$\langle\langle J_eJ_e, J_gJ_g|R^{(1)}(s)|J_eJ_e, J_eJ_g\rangle\rangle = -i(f_{J_g}\Omega_{eg}/2)\left[(s+\gamma)(s+\gamma/2-i\Delta)+(f_{J_g}\Omega_{eg}/2)^2\right]^{-1}. \quad \text{(A18)}$$

The problem of calculating the resolvent operator has, therefore, been reduced to inverting tridiagonal matrices $Z^{(l)}(s)$. For resonance fluorescence and probe spectra, we need only to be concerned about $Z^{(0)}(s)$ and $Z^{(1)}(s)$. They are given explicitly by

$$Z^{(0)}(s) = \begin{pmatrix} x^{(0)}_{-J_g} & y^{(0)}_{-J_g+1} & & & & \\ z^{(0)}_{-J_g} & x^{(0)}_{-J_g+1} & y^{(0)}_{-J_g+2} & & & \\ & z^{(0)}_{-J_g+1} & \ddots & \ddots & & \\ & & \ddots & \ddots & & y^{(0)}_{J_g} \\ & & & & z^{(0)}_{J_g-1} & x^{(0)}_{J_g} \end{pmatrix}, \quad \text{(A19)}$$

where

$$x^{(0)}_m(s) = s\left\{(s+\gamma)[(s+\gamma/2)^2+\Delta^2]+(s+\gamma/2)f_m^2\Omega_{eg}^2\right\}+(\gamma/2)(s+\gamma/2)f_m^2[1-(2J_e+1)f_m^2]\Omega_{eg}^2, \quad \text{(A20)}$$

$$y^{(0)}_m(s) = -(\gamma/2)(s+\gamma/2)(2J_e+1)f_m^2h_m^2\Omega_{eg}^2, \quad \text{(A21)}$$

$$z^{(0)}_m(s) = y^{(0)}_{-m}(s), \quad \text{(A22)}$$

and

$$Z^{(1)}(s) = \begin{pmatrix} x^{(1)}_{-J_g+1} & y^{(1)}_{-J_g+1} & & & & \\ z^{(1)}_{-J_g+1} & x^{(1)}_{-J_g+2} & y^{(1)}_{-J_g+2} & & & \\ & z^{(1)}_{-J_g+2} & \ddots & \ddots & & \\ & & \ddots & \ddots & & y^{(1)}_{J_g-1} \\ & & & & z^{(1)}_{J_g-1} & x^{(1)}_{J_g} \end{pmatrix}, \quad \text{(A23)}$$

$$x^{(1)}_m(s) = \left[s(s+i\Delta+\gamma/2)-\left(f_m^2-f_{m-1}^2\right)(\Omega_{eg}/2)^2\right]\left[(s+\gamma)(s-i\Delta+\gamma/2)-\left(f_m^2-f_{m-1}^2\right)(\Omega_{eg}/2)^2\right]$$
$$+(s+\gamma/2)^2f_m^2\Omega_{eg}^2-(\gamma/2)(s+\gamma/2)(2J_e+1)f_m^2f_{m-1}^2\Omega_{eg}^2, \quad \text{(A24)}$$

$$y^{(1)}_m(s) = -(\gamma/2)(s+\gamma/2)(2J_e+1)f_mf_{m+1}h_mh_{m+1}\Omega_{eg}^2, \quad \text{(A25)}$$

$$z^{(1)}_m(s) = y^{(1)}_{-m}(s). \quad \text{(A26)}$$

For any finite J_g, the inversion of $Z^{(l)}(s)$ can in principle be carried out analytically. However, the resulting analytic expressions for the spectra (valid for arbitrary detuning and Rabi frequency) are usually so complicated that they do not have much advantage over numerical results, which can be obtained very easily and efficiently.

For our goals in this paper, $|J_1m_1, J_2m_2\rangle\rangle$ turns out to be the most convenient basis set for the Liouville space. But there are definitely other options. One of them is the basis set built out of the states which diagonalize $H_A^R + H_{AL}^R$, i.e. the dressed states. Another one is the irreducible tensor representation [9,23,40], which may be useful in the presence of collisions [23].

APPENDIX B: S EXPANSION OF INTEGRATED RATES

An important characteristic of the integrated rates W, $W_{\rm coh}$, $W_{\rm inc}$, $W_{\rm inc}^{\Delta m=0}$, and $W_{\rm inc}^{|\Delta m|=1}$ is that when scaled

by γ, their dependences on Δ, Ω_{eg}, and γ are through the saturation parameter S only. From Eqs. (38), (42), (43), (45), and (46), we have

$$W/\gamma = \tfrac{1}{2}S(1+S)^{-1} \quad \text{(B1)}$$
$$= \tfrac{1}{2}(S - S^2 + \cdots) ,$$
$$W_{\rm coh}/\gamma = [(2J_e+1)g_s/2]S(1+S)^{-2}$$
$$= [(2J_e+1)g_s/2](S - 2S^2 + \cdots) , \quad \text{(B2)}$$
$$W_{\rm inc}/\gamma = \tfrac{1}{2}\{[1-(2J_e+1)g_s]S + S^2\}(1+S)^{-2}$$
$$= \tfrac{1}{2}\{[1-(2J_e+1)g_s]S$$
$$+[2(2J_e+1)g_s - 1]S^2 + \cdots\} , \quad \text{(B3)}$$
$$W_{\rm inc}^{\Delta m=0}/\gamma = [(2J_e+1)/(2g_s)][(g_4 - g_s^2)S$$
$$+g_4 S^2](1+S)^{-2}$$
$$= [(2J_e+1)/(2g_s)][(g_4 - g_s^2)S$$
$$+(2g_s^2 - g_4)S^2 + \cdots) , \quad \text{(B4)}$$
$$W_{\rm inc}^{|\Delta m|=1}/\gamma = \{[g_s - (2J_e+1)g_4]/(2g_s)\}S(1+S)^{-1}$$
$$= \{[g_s - (2J_e+1)g_4]/(2g_s)\}$$
$$\times(S - S^2 + S^3 - \cdots) . \quad \text{(B5)}$$

For a TLS ($J_g = 0$ and $J_e = 1$), $1-(2J_e+1)g_s = 0$ and the S expansion for $W_{\rm inc}$ starts at S^2 term. This is intimately related to the fact that in the limit of weak coupling, incoherent scatterings by a TLS can happen only through multiple (pump) photon processes [31]. For transitions with a degenerate ground state, the S expansion for $W_{\rm inc}$ starts with a S term which is the contribution from the spontaneous Raman scattering and the incoherent Rayleigh scattering, both involving only a single pump photon.

Equations (B1)–(B5) can also be expanded in power series of $1/S$, which can be useful in the limit of strong coupling. We merely note that all integrated rates approach some constant values in the limit of $S \gg 1$. And the spectrum becomes purely incoherent.

In Sec. II B, the limit of weak coupling is characterized by $S \to 0$. It is desirable to know more precisely how small S has to be for $W_{0,\rm inc}(\omega)$ to be dominated by the incoherent Rayleigh scattering and for $W_1(\omega)$ to be dominated by the spontaneous Raman scattering. These criteria can be obtained by comparing the magnitudes of the S^2 term and the S term in the S expansions of $W_{\rm inc}^{\Delta m=0}/\gamma$ and $W_{\rm inc}^{|\Delta m|=1}/\gamma$. Defining S_0 and S_1 as the values of S for which the S^2 term and the S term in $W_{\rm inc}^{\Delta m=0}/\gamma$ and $W_{\rm inc}^{|\Delta m|=1}/\gamma$, respectively, become equal, we have

$$S_1 = 1 , \quad \text{(B6)}$$
$$S_0 = \left|(g_4 - g_s^2)/(2g_s^2 - g_4)\right| . \quad \text{(B7)}$$

The condition for $W_1(\omega)$ to be dominated by spontaneous Raman scatterings is, therefore, $S \ll S_1 = 1$. Figures 23(a) and 23(b) show the values of S_0 for $\Delta J = 0$ and $\Delta J = 1$ types of transitions respectively [25]. The condition for $W_{0,\rm inc}(\omega)$ to be dominated by incoherent Rayleigh scatterings is $S \ll S_0$, which yields very different conditions depending on ΔJ. For $\Delta J = 0$ type of transitions, $S \ll S_0$ is roughly equivalent to $S_0 \ll 1$. For $\Delta J = 1$ type of transitions, however, S has to be much smaller to satisfy $S \ll S_0$. For example, for a 2 to 3 transition, $S \ll S_0$ requires $S \ll 1.66 \times 10^{-2}$. This condition is however not as important as it seems if we recall that $W_0(\omega)$ is only a small fraction of $W(\omega)$ for $\Delta J = 1$ type of transitions. Taking this into account, the limit of weak coupling corresponds roughly to $S \ll 1$.

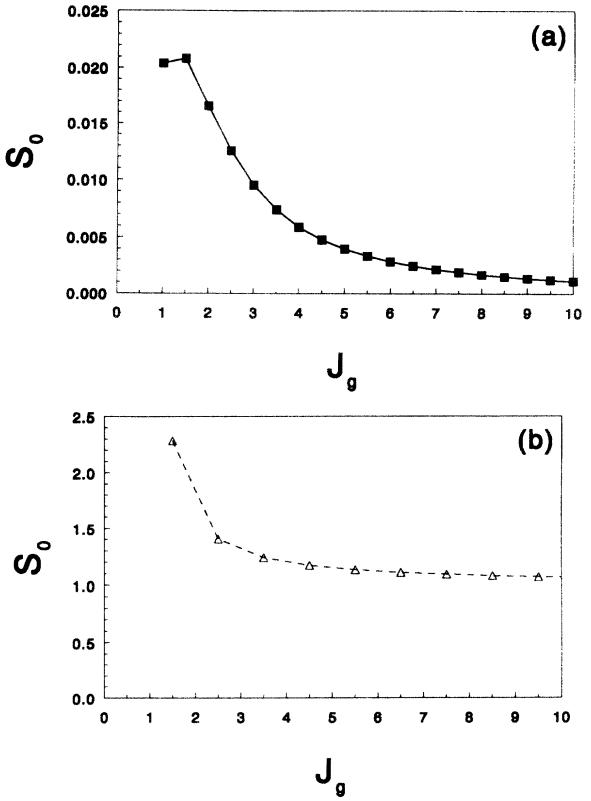

FIG. 23. S_0 (defined in Appendix B) vs J_g for (a) $\Delta J = 1$ type of transitions and (b) $\Delta J = 0$ type of transitions.

APPENDIX C: THE LIMIT OF WEAK COUPLING

In the limit of weak coupling, the resonance fluorescence is nonzero only in the region of $|\omega - \omega_L| \ll \gamma$, where Eqs. (A20) and (A21) and Eqs. (A24) and (A25) become, respectively,

$$x_m^{(0)}(s = -i(\omega - \omega_L)) \approx \gamma[(\gamma/2)^2 + \Delta^2]s + \gamma^2[1-(2J_e+1)f_m^2](f_m\Omega_{eg}/2)^2 , \quad \text{(C1)}$$
$$y_m^{(0)}(s = -i(\omega - \omega_L)) \approx -\gamma^2(2J_e+1)h_m^2(f_m\Omega_{eg}/2)^2 , \quad \text{(C2)}$$

and

$$x_m^{(1)}(s=-i(\omega-\omega_L)) \approx \gamma[(\gamma/2)^2+\Delta^2]s + i\gamma\Delta(f_m^2-f_{m-1}^2)(\Omega_{eg}/2)^2 + \gamma^2(1/2)\Big\{ f_m^2[1-(2J_e+1)f_m^2] + f_{m-1}^2[1-(2J_e+1)f_{m-1}^2] + (2J_e+1)(f_m^2-f_{m-1}^2)^2 \Big\}(\Omega_{eg}/2)^2 , \quad \text{(C3)}$$

$$y_m^{(1)}(s=-i(\omega-\omega_L)) \approx -\gamma^2(2J_e+1)f_m f_{m+1} h_m h_{m+1}(\Omega_{eg}/2)^2 . \quad \text{(C4)}$$

The determinant of $Z^{(0)}(s)$ has in this case $(2J_g+1)$ roots. One of them is $s=0$ which corresponds to the coherent Rayleigh scattering. Other $2J_g$ roots determine the line shape for the incoherent Rayleigh scattering. From Eqs. (C1) and (C2), it is obvious that all these roots obey

$$s \propto \gamma\Omega_{eg}^2[\Delta^2+(\gamma/2)^2]^{-1} . \quad \text{(C5)}$$

The incoherent Rayleigh resonance is, therefore, much narrower than γ in the limit of either weak field or large detuning. It is generally difficult, for arbitrary J_g, to separated the incoherent Rayleigh scattering into $2J_g$ terms corresponding to each of the $2J_g$ roots. There is however no good physical reason to do so anyway. They always overlap, and as pointed out in Sec. II B, we cannot assign the incoherent Rayleigh scattering to individual m states. It is something that belongs to all m states as a whole.

The determinant of $Z^{(1)}(s)$ has, in the region $|s| \ll \gamma$, $2J_g$ roots, corresponding to $2J_g$ spontaneous Raman resonances. From Eqs. (C3) and (C4) it is obvious that all $2J_g$ roots, both their real and imaginary parts, are proportional to Ω_{eg}^2. It is also clear that spontaneous Raman resonances can become well separated in the limit of large detuning. In fact, since the differences between the diagonal terms of $Z^{(1)}(s)$ depend on $1/\Delta$ while the off-diagonal terms depend on $1/\Delta^2$, the off-diagonal terms can be completely ignored for sufficiently large detuning. We have then (recall the definition $Y^{(1)}(s) \equiv [Z^{(1)}(s)]^{-1}$)

$$\langle m'|Y^{(1)}(-i(\omega-\omega_L))|m\rangle = \gamma^{-1}[(\gamma/2)^2+\Delta^2]^{-1}\Big\{ -i[(\omega-\omega_L)-\delta_m]+\eta_m \Big\}^{-1} \times \delta_{m'm} , \quad \text{(C6)}$$

where

$$\delta_m = \Delta(f_m^2-f_{m-1}^2)(\Omega_{eg}/2)^2[\Delta^2+(\gamma/2)^2]^{-1} , \quad \text{(C7)}$$

$$\eta_m = \gamma(1/2)\Big\{ f_m^2[1-(2J_e+1)f_m^2] + f_{m-1}^2[1-(2J_e+1)f_{m-1}^2] + (2J_e+1)(f_m^2-f_{m-1}^2)^2 \Big\}(\Omega_{eg}/2)^2 \times [\Delta^2+(\gamma/2)^2]^{-1} . \quad \text{(C8)}$$

Substituting Eq. (C6) into Eqs. (A13), (A14), and (9), we obtain Eq. (53).

δ_m and η_m are, respectively, the frequency shift and the width of the spontaneous Raman transition from $m_g = m$ to $m_g = m-1$. δ_m could have been derived from the usual wave function perturbation theory. But the same cannot be said about η_m. The first two terms in Eq. (C8) represent the average of spontaneous Raman scattering rates out of $m_g = m$ and $m_g = m-1$ states, which is the linewidth I was originally anticipating for spontaneous Raman resonances. It turns out however that Rayleigh scattering can also contribute to the line width in a subtle fashion. We attribute the last term in Eq. (C8) to the incoherent Rayleigh scattering, since it would have been be zero if $|f_m|$ was independent of m.

For small detunings where spontaneous Raman resonances overlap, writing the spectrum as the sum of the terms corresponding to each individual roots is not very meaningful, and is also much more difficult.

[1] J. Dalibard and C. Cohen-Tannoudji, J. Opt. Soc. Am. B **6**, 2023 (1989).
[2] P.J. Ungar, D.S. Weiss, E. Riis, and S. Chu, J. Opt. Soc. Am. B **6**, 2058 (1989).
[3] D.S. Weiss, E. Riis, Y. Shevy, P.J. Ungar, and S. Chu, J. Opt. Soc. Am. B **6**, 2072 (1989).
[4] E. Bonderup and K. Molmer, J. Opt. Soc. Am. B **6**, 2125 (1989).
[5] C.I. Westbrook *et al.*, Phys. Rev. Lett. **65**, 33 (1990).
[6] G. Grynberg, M. Vallet, and M. Pinard, Phys. Rev. Lett. **65**, 701 (1990).
[7] J.W.R. Tabosa, G. Chen, Z. Hu, R.B. Lee, and H.J. Kimble, Phys. Rev. Lett. **66**, 3245 (1991).
[8] D. Grison, B. Lounis, C. Salomon, J.Y. Courtois, and G. Grynberg, Europhys. Lett. **15** 149 (1991).
[9] P.R. Berman, Phys. Rev. A **43**, 1470 (1991).

[10] Y. Castin and J. Dalibard, Europhys. Lett. **14**, 761 (1991).
[11] P. Marte, P. Zoller, and J.L. Hall, Phys. Rev. A **44**, R4118 (1991).
[12] P.S. Jessen *et al.*, Phys. Rev. Lett. **69**, 49 (1992).
[13] B. Lounis, J.Y. Courtois, P. Verkerk, C. Salomon, and G. Grynberg, Phys. Rev. Lett. **69**, 3029 (1992).
[14] V. Finkelstein, P.R. Berman, and J. Guo, Phys. Rev. A **45**, 1829 (1992).
[15] J.Y. Courtois and G. Grynberg, Phys. Rev. A **46**, 7060 (1992); **48**, 1378 (1993).
[16] P. Marte, R. Dum, R. Taieb, P.D. Lett, and P. Zoller, Phys. Rev. A **47**, 1378 (1993).
[17] J. Guo and P.R. Berman, Phys. Rev. A **47**, 4128 (1993); **48**, 3225 (1993).
[18] R. Taieb, P. Marte, R. Dum, and P. Zoller, Phys. Rev. A **47**, 4986 (1993).
[19] P. van der Straten *et al.*, Phys. Rev. A **47**, 4160 (1993).
[20] P.R. Berman, G. Rogers, and B. Dubetsky, Phys. Rev. A **48**, 1506 (1993).
[21] B. Gao, Phys. Rev. A **49**, 3391 (1994).
[22] D. Polder and M.F.H. Schuurmans, Phys. Rev. A **14**, 1468 (1976).
[23] J. Cooper, R.J. Ballagh, and K. Burnett, Phys. Rev. A **22**, 535 (1980).
[24] B.R. Mollow, Phys. Rev. **188**, 1969 (1969).
[25] In the context of this paper, $\Delta J = 0$ type of transitions refer to transitions with $J_e = J_g$ and equal to a half integer; $\Delta J = 1$ type of transitions refer to transitions with $J_e = J_g + 1$. For linearly polarized laser field, there is no steady-state resonance fluorescence in other cases.
[26] B. Gao, Phys. Rev. A **48**, 2443 (1993).
[27] M. Trippenbach, B. Gao, and J. Cooper, Phys. Rev. A **45**, 6555 (1992).
[28] C. Cohen-Tannoudji, in *Frontiers in Laser Spectroscopy*, edited by R. Balian, S. Haroche, and S. Liberman (North-Holland, Amsterdam, 1977), p. 3.
[29] $W_{\mathbf{e}}(\omega, \theta, \phi)$ depends on the angles only through the polarization vector $\mathbf{e}$. For fixed $\mathbf{e}$, $W_{\mathbf{e}}(\omega, \theta, \phi)$ is independent of the angles θ and ϕ.
[30] See e.g., M. Rotenberg *et al.*, *The 3-j and 6-j symbols* (MIT, Cambridge, 1959).
[31] C. Cohen-Tannoudji, J. Dupont-Roc, and G. Grynberg, *Atom-Photon Interactions* (John Wiley and Sons, New York, 1992).
[32] See e.g., I. Lindgren and J. Morrison, *Atomic Many-Body Theory* (Springer-Verlag, Berlin, 1982).
[33] W.R. Johnson, M. Idress, and J. Sapirstein, Phys. Rev. A **42**, 3218 (1987).
[34] L. Shabanova, Yu. Monukov, and A. Khlyustalov, Opt. Spektrosk. **47**, 3 (1979) [Opt. Spectrosc. (USSR) **47**, 1 (1979)].
[35] M. Wilkens, Phys. Rev. A **47**, 671 (1993); **49**, 570 (1994).
[36] C. Baxter, M. Babiker, and R. Loudon, Phys. Rev. A **47**, 1278 (1993); V.E. Lembessis, M. Babiker, C. Baxter, and R. Loudon, *ibid.* **48**, 1594 (1993).
[37] K. Burnett, J. Cooper, R.J. Ballagh, and E.W. Smith, Phys. Rev. A **22**, 2005 (1980).
[38] A. Ben-Reuven, Adv. Chem. Phys. **33**, 235 (1975).
[39] U. Fano, in *Lectures on the Many-Body Problem,* Vol. 2, edited by E.R. Caianiello (Academic Press, New York, 1964), p. 217.
[40] A. Omont, Prog. Quantum Electron. **5**, 69 (1977).